BRNO UNIVERSITY OF TECHNOLOGY
VYSOKÉ UČENÍ TECHNICKÉ V BRNĚ

FACULTY OF INFORMATION TECHNOLOGY
FAKULTA INFORMAČNÍCH TECHNOLOGIÍ

DEPARTMENT OF INTELLIGENT SYSTEMS
ÚSTAV INTELIGENTNÍCH SYSTÉMŮ

DETECTION OF PATHOLOGICAL FINDINGS IN VIDEOS FROM BRONCHIAL PATHWAYS
DETEKCIA PATOLÓGIÍ ZO ZÁZNAMOV Z BRONCHIÁLNYCH CIEST

BACHELOR'S THESIS
BAKALÁŘSKÁ PRÁCE

AUTHOR **MARTIN NOVOTNÝ MLINÁRCSIK**
AUTOR PRÁCE

SUPERVISOR **prof. Ing. MARTIN DRAHANSKÝ, Ph.D.**
VEDOUCÍ PRÁCE

BRNO 2021

Department of Intelligent Systems (DITS)   Academic year 2021/2022

Bachelor's Thesis Specification

||||||||||||||||||||||
24849

Student: **Novotný Mlinárcsik Martin**

Programme: Information Technology

Title: **Detection of Pathological Findings in Videos from Bronchial Pathways**

Category: Image Processing

Assignment:

1. Study the literature on image recognition in OpenCV and human respiratory diseases.
2. Propose an algorithmic solution for detection of pathological findings in bronchial tubes.
3. Implement the proposed solution from the previous point.
4. Summarize the achieved results and discuss possible extensions or improvements.

Recommended literature:

- BRADSKI, G. R., & KAEHLER, A. (2008). Learning OpenCV: computer vision with the OpenCV library. Sebastopol, CA, O'Reilly.
- Zhou, S. K. (2016). Introduction to Medical Image Recognition, Segmentation, and Parsing. Medical Image Recognition, Segmentation and Parsing, 1-21. doi:10.1016/b978-0-12-802581-9.00001-9
- ZÁMEČNÍK, Josef, ed. Patologie. První vydání. Praha: LD Prager Publishing, 2019. 3 svazky (lxxiii, 915, xciv stran).

Requirements for the first semester:

- Items 1 and 2.

Detailed formal requirements can be found at https://www.fit.vut.cz/study/theses/

Supervisor: **Drahanský Martin, prof. Ing., Dipl.-Ing., Ph.D.**

Head of Department: Hanáček Petr, doc. Dr. Ing.

Beginning of work: November 1, 2021

Submission deadline: May 11, 2022

Approval date: May 9, 2022

Abstract

The aim of this work is a detection of lung pathologies in videos from bronchial airways. Videos of bronchial passages, created by inserting a bronchoscope into a patient, are used as an input. Afterwards, individual frames are processed in a way that pathologies are color separated from non-pathological background as dark spots. These dark spots are then analyzed by a Blob Detector, which will mark these as pathological and highlight them in the output image.

Abstrakt

Cieľom tejto práce je detekcia pľúcnych patológií na záznamoch z bronchiálnych ciest. Vstupom je záznam bronchiálnych ciest vytvorený bronchoskopom, ktorý je zavedený do tela pacienta. Následne sú jednotlivé snímky spracované tak, aby boli patológie farebne separované od nepatologického pozadia. Na tieto tmavé miesta je následne použitý nástroj Blob Detector, ktorý tmavé miesta spracuje a vyhodnotí ako patologické. Tieto miesta sú následne zvýraznené na výstupe.

Keywords

Klíčová slova

Reference

Rozšířený abstrakt

Táto práca sa zaoberá analýzou záznamov z bronchiálnych ciest, pričom na týchto záznamoch vyhľadavá pľúcne patológie. V modernej dobe existujú viaceré medicínske možnosti zobrazenia pľúc a pľúcnych patológií, medzi ktoré radíme napríklad pľúcnu rádiografiu, výpočetnú tomografiu, zobrazovanie pomocou magnetickej rezonancie, jednofotónovú emisnú tomografiu, pozitrónovú emisnú tomografiu alebo zobrazovanie pomocou ultrazvuku. Avšak tieto zobrazovacie metódy sú často zdraviu škodlivé a ich časté vykonávanie nie je možné, alebo ich miera zobrazenia nie je dostatočné pre presné určenie typu a miesta patológie. V prípade zobrazovania pomocou magnetickej rezoznancie alebo výpočetnej tomografie sú potrebné drahé, špecializované zariadenia, ktoré pre svoju funkčnosť potrebujú medicínskych technikov. Táto práca prezentuje spôsob zobrazenia v blízkom infračervenom spektre za pomoci bronchoskopu, ktorý je v porovnaní s vyššie spomenutými prístrojmi lacnejšou a prístupnejšou alternatívou.

Do bronchiálnych ciest je zavedený flexibilný bronchoskop spolu s elektroluminiscenčnou diódou, ktorá vyžaruje svetlo v blízkom infračervenom spektre. Toto žiarenie je schopné transluminovať pľúcne tkanivo do väčšej hĺbky ako svetlo vo viditeľnom spektre a umožňuje tak spozorovať patológie, ktorá sa vyjavia ako tmavé miesta, kvôli ich odlišnej bunkovej štruktúre. Tieto záznamy sú potom spracované programom, ktorý je opísaný v tejto práci. Keďže elektroluminiscenčnú diódu, použitú pre osvetlenie priestoru bronchiálnych ciest, je možné brať ako bodový zdroj svetla, sú vstupné snímky často nerovnomerne osvetlené. Algoritmus spracováva snímky vstupného videa jednotlivo za sebou, pričom na začiatku vykonáva normalizáciu osvetlenia v scéne. Táto normalizácia sa vykonáva na základe odhadu priemeru jasu a odhadu rozptylu zo vstupného snímku za cieľom uniformácie jasu v jednotlivých lokálnych častiach snímku. Výstupom normalizácie je čistejší obraz, na ktorom je možné bližšie a lepšie rozlíšiť štruktúry bronchiálnych ciest. Taktiež výsledkom normalzácie je farebná separácia možných patológií, ktoré budú odlíšené od nepatologického pozadia. Na výsledný obraz je ešte použitá funkcionalita CLAHE, alebo kontrastom limitovaná adaptívna ekvalizácia histogramu, ktorá zvýši kontrast medzi tmavými a svetlými miestami v snímku. Na detekciu patológií je použitý nástroj BlobDetector, ktorý na základe prednastavených parametrov zvýrazňuje tmavé miesta v snímku. Po algoritmoch pre spracovanie obrazu je výsledný snímok zobrazený v aplikácií, pričom je zobrazený bok po boku so vstupným snímkom. Užívateľ si môže kedykoľvek pozastaviť proces spracovania obrazu a potom ho znovu spustiť. Pri zvýraznení patológie je snímok s patológiou uložený do adresára. Program poskytuje funkcionalitu pre zobrazenie týchto uložených snímkov. Pri otvorení tohto nového okna aplikácie môže užívateľ zvoliť konkrétny adresár, v ktorom sú uložené snímky podľa náznov vstupných videí. Obsah tohto adresára bude potom viditeľný v zozname, pričom jednotlivé snímky budú viditeľné v spomenutom okne.

Program bol otestovaný na limitovanom datasete. Program funguje relatívne spoľahlivo pri snímkoch, na ktorých bola kamera zaostrená a snímok nebol preexponovaný. V týchto prípadoch bola scéna správne normalizovaná a na snímkoch je možné rozlíšiť jednotlivé štruktúry bronchiálnych ciest. V prípadoch, kedy bola scéna preexponovaná, miesta dochádzalo k až miernemu ztmaveniu tmavých miest zo vstuného snímku, čo miestami spôsobovalo chybnú detekciu patológií. Najproblémovejšie sú preexponované snímky s nezaostrenou kamerou, kde sa jednotlivé nevýrazné štruktúry zlievajú do väčších celkov. Toto chýbajúce rozlíšenie spôsobuje problémy pri normalizácií, kde sú tieto tmavé zliate celky až prílišne ztmavené, pričom spôsobujú chybnú detekciu patológií.

Detection of pathological findings in videos from bronchial pathways

Declaration

I declare that this bachelor's thesis as an original author's work under the supervision of Prof. Ing. Martin Drahanský Ph.D. All relevant information sources used for this thesis are properly cited in the list of references.

<div align="right">

. . . .
Martin Novotný Mlinárcsik
May 10, 2022

</div>

Contents

Chapter 1

Introduction

Image recognition and image processing are topics that have been largely popularized in recent years. From biometric fingerprint scanners and face detectors to the rise of autonomous, self-driving automobiles, image processing is being introduced to the lives of ordinary people now more than ever and plays a vital role in a number of industries, where precise and fast object recognition is critical. Especially in medicine, image recognition is an important asset to medical personnel, as many parts of a human body are inaccessible by conventional means and therefore require specialized apparatuses to be accessed. In modern medicine, image processing is used in various fields, some of which are used to diagnose a wide range of pathologies - computed tomography, magnetic resonance, nuclear medicine, and many others. However, the use of imaging devices is oftentimes done under time constrictions, as patients undergoing such procedures are under the effect of medically induced coma or are at risk of tissue damage caused by the use of ionizing radiation. Therefore, image processing must be implemented in a way that allows swift collection of information.

Some of such devices, in our case, video cameras, are also limited in terms of their capabilities due to their restricted size. In addition to size restrictions, these devices usually operate under low light conditions, which make the resultant image significantly more difficult to analyze by humans. Therefore, we can utilize computing techniques to enhance these images and highlight areas of interest.

The aim of this thesis is to propose a solution that would enhance a video feed coming from a camera in a patient's bronchial airways and subsequently highlight areas of potential pathologies. It aims to assist medical professionals with a diagnosis of lung and bronchial pathologies without the need for surgical intervention or exposure to harmful radiation.

In this work, Chapter 2 offers a brief overlook of the basics of lung anatomy and physiology, as well as types of malignant tumors. Chapter 3 talks about modern medical imaging systems, their functionality, and their benefits. Chapter 4 discusses the experimental image acquisition setup used for this work. Chapter 5 describes the proposed solution used in this work. Chapter 6 discusses the testing of the algorithm.

Chapter 2

Medicine

This chapter discusses the anatomy and physiology of human lungs, as well as malign and benign tumors that affect various parts of the organ.

2.1 Lungs

Lungs are a paired organ that handles gas exchange between a human body and its environment, as they are responsible *respiration* - oxygen blood saturation and the expulsion of carbon dioxide. If sustained damage, the patient to suffer from insufficient oxygen saturation, causing depressed mental activity, reduced muscle strength, and potential brain failure.

2.1.1 Anatomy

Human respiratory system is divided into 2 zones - the **conducting zone** and the **respiratory zone**. The conducting zone does not take part in gas exchange and only serves as a pathway to the respiratory zone.

The lungs are placed on the left and the right side of the thoracic cage. Their bottom base is in direct contact with the diaphragm, which assists in pulmonary ventilation. Nerves, arteries, veins, bronchi, and lymph vessels enter the lung via an anatomical structure called **hilum**, which is situated roughly in the middle of each lung from the medial view. In addition to the circulation of bodily fluids, these structures also help with the suspension of the lungs.

The right lung **(pulmo dexter)** consists of 3 lobes - superior, middle, and inferior lobe, while the left lung **(pulmo sinister)** only consists of 2 lobes - superior and inferior. This is due to the fact that the heart tilts to the left, for which the left lung has to accommodate. Every lobe is further segmented into bronchopulmonary segments.

Air passes into the lungs from the upper air passages into the lungs via the trachea. The trachea and subsequent bronchi are formed by multiple U-shaped segments made of cartilage, connected by smooth connective tissue. The trachea bifurcates into two main bronchi - shorter, wider right bronchus **(bronchus principalis dexter)** and longer, narrower left bronchus **(bronchus principalis sinister)**, which enter the lungs by the hilum. For each pulmonary lobe, a separate secondary bronchus branches out from the primary bronchus - 3 for the right lung and 2 for the left lung. As every pulmonary lobe further segments into smaller bronchopulmonary lobes, each secondary bronchus separates into tertiary bronchi - 10 for the right lung and 9 for the left lung. From these tertiary bronchi stem smaller

bronchioli, which lack the characteristic cartilage structure of bronchi. Instead, bronchioli are held open by the tension of the surrounding tissue. The conducting zone of the human respiratory system ends with **terminal brionchioli**. From these bronchi emerge **respiratory bronchi**, which are the beginning of the respiratory zone of the human respiratory system.

The most basic functional part of the lungs and the respiratory zone is the **alveoli**. Alveoli are surrounded by a dense web way of blood vessels, which bring deoxygenated blood to absorb oxygen molecules from the alveoli. Alveoli are comprised into **alveolar sacks**, which are connected to the respiratory bronchi by the **alveolar ducts**. [21]
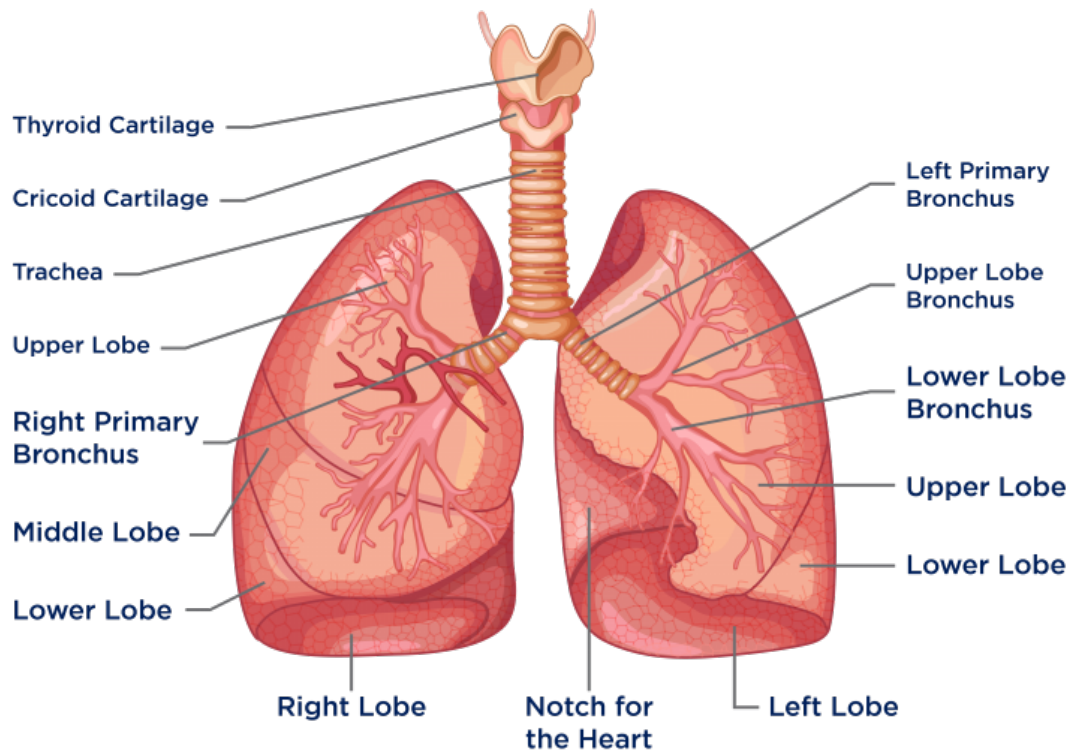

Figure 2.1: Anatomy of lungs [1].

2.1.2   Physiology

The surfaces of each lung are covered by a thin membrane called **pleura**, comprised of 2 parts. The inner surface is covered by a **visceral pleura**, which then, at the hilum, transitions into a **parential pleura** that covers the outer surface, facing the thoracic cage, mediastinum, and diaphragm. In between these membranes lies a **pleural cavity**, filled with **pleural fluid**. As the lungs expand and compress during pulmonary ventilation, the pleural fluid provides a reduction of surface tension between the two membranes. Because the membrane is porous, pleural fluid is also present on the surface of the parietal pleura, allowing the lungs to slide freely on the thoracic cage while maintaining surface tension so

that the lungs expand together with the thoracic cavity and stay connected to it. If the volume of pleural fluid exceeds the limit, the excess is drained by lymphatic vessels.

In the moment of inhalation, the diaphragm contracts downwards and increases the volume of the thoracic cage. Because of the volume increase, the atmospheric pressure inside the respiratory system decreases, and the air moves into the lungs and fills the alveoli. The alveolar air is different from the atmospheric air as their compositions vary, as carbon dioxide and oxygen are being diffused at all times, and the fact that undamaged lungs will at all times maintain a certain volume of air. During times of heightened demand for oxygen, the body can contract **external intercostal muscles**, located between ribs, and expand the rib cage even more.

The rate of the oxygen diffusion depends of multiple factors, mainly:

- Partial pressure of oxygen (PO_2)

- Partial pressure of carbon dioxide (PCO_2)

Additional factors:

- Tissue pH level

- Amount of 2,3-Bisphosphoglyceric acid (2,3-DPG)

- Tissue temperature

High partial oxygen pressure in alveoli allows for easier bounding to hemoglobin, while low partial pressure in tissues allows the oxygen molecules to escape the hemoglobin cell. The **oxygen dissociation curve** moves to the right as the temperature in active tissues rises up, the concentration of oxygen lowers, and the concentration of carbon dioxide rises. 2,3-DPG is a metabolic byproduct that interferes with oxygen diffusion and also shifts the dissociation curve to the right. As a result of the curve's shift, the affinity of hemoglobin towards the oxygen falls, and oxygen molecules are able to separate from the hemoglobin cells.

On the other hand, in the lungs, the partial pressure of oxygen is much higher due to the pulmonary ventilation, which supplies the alveoli with fresh air. As lungs are not an act as, for example, muscles, temperature, and levels of 2,3-DPG are lower. As a result, the dissociation curve shifts to the left, increasing the affinity of red blood cells towards the oxygen and aiding in oxygenation, while carbon dioxide moves to the alveoli, from where it is exhaled. [26, 18, 27]
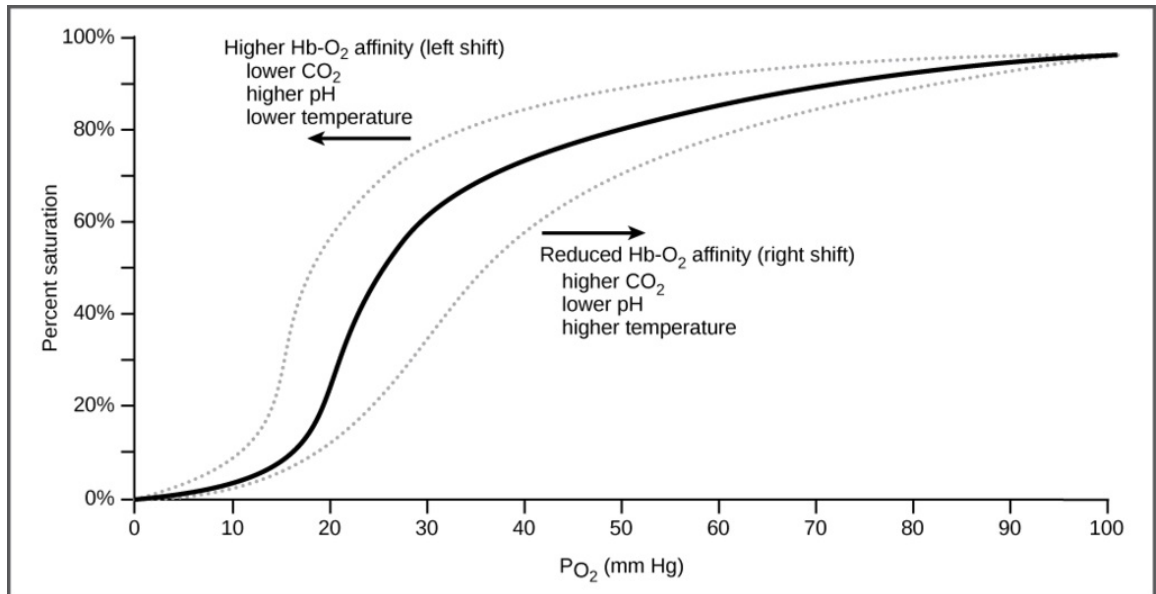
Figure 2.2: Oxygen dissociation curve [9].

2.2 Lung cancer

Most of lung tumors are classified as **carcinomas**, as carcinomas arise from epithelial cells. Carcinomas are malignant and benign types of tumors are rare in lung tissue. We distinguish 2 different types of lung carcinomas:

- Small cell lung cancer (SCLC)

- Non-small cell lung cancer (NSCLC)

Small lung cell carcinomas are a more aggressive variant, where surgical removal of malignant tissue is impossible, as, at the time of diagnosis, the primary malignant tumor may have metastasized and spread into surrounding lymph nodes or organs. Small lung cell carcinomas account for roughly 20% of lung cancers.

Non-small lung cell carcinomas tend to be less aggressive than small cell carcinomas with much more positive prognoses. Removal of malignant tissue is vital, as they are less sensitive to chemotherapy and radiotherapy. They make up for roughly 80% of all lung cancers.

2.2.1 Adenocarcinoma

Adenocarcinomas are malignant tumors of glandular epithelial tissues. Adenocarcinoma can emerge from already present adenoma that undergoes dysplastic molecular changes or can create flat dysplastic areas. Dysplasia of glandular tissue is characterized by atypically enlarged cell nuclei or relocation of the nucleus from the basal area of a cell to its center.

Low-grade adenocarcinomas have high differentiation, where transitions from the original tissue can be seen. In the later stages, when adenocarcinomas become less differentiated, they start to solidify and lose their ability to create lumens, and they start to dissociate. When adenocarcinomas become dissociated, they lose their cohesion and can spread around

the tissue surface. Cells that retain their mucin production ability are called **signet cell rings**

In the lungs, the precancerous state of adenocarcinomas is called the **atypic adenomatous hyperplasia**. Tumors can vary from a few centimeters in diameter to tumors that span the entire pulmonary lobe. Lung adenocarcinomas range from white to gray in color and can be pliable depending on the level of mucin production. [29, 28]
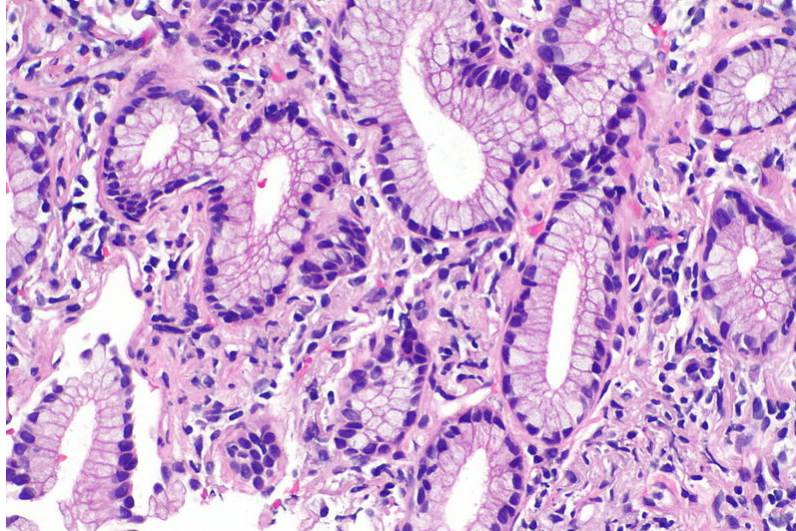

Figure 2.3: Lung adenocarcinoma [8].

2.2.2 Squamous cell carcinoma

Squamous cell carcinomas usually emerge from squamous epithelial cells. Low-grade squamous cell carcinomas closely resemble non-cancerous squamous epithelium, where towards the upper layers, tumor cells are narrower and can keratinize. In high-grade carcinomas, low differentiation causes problems with tumor identification and a more suitable area for bioptic sample, as microscopy might be ineffective in differentiating cell types.

In the lungs, chronic irritation of bronchial epithelial cells can lead to continuous **metaplasia** of epithelial linings, as **pseudostratified columnar epithelium** transforms into squamous epithelium, which can later develop **dysplasia**. Dysplasia describes a tissue with the presence of abnormal cells. Squamous cell carcinomas most usually occur in the main and segmental bronchi. Metastases occur in advanced stages. The rate of spreading of squamous cell carcinomas depends on their localization and differentiation. In the lungs, these carcinomas resemble white or gray mass. [29, 28]

2.2.3 Neuroendocrine neoplasm

Neuroendocrine tumors show both endocrine and neuronal differentiation. Among the types that are commonly found in the lungs, all are highly malignant. We distinguish three types of neuroendocrine tumors:

- **Neuroendocrine tumors (NET)** are usually well-differentiated, with regular polynomial cells that create solid cell nests. They include both low-grade and high-grade malignities.
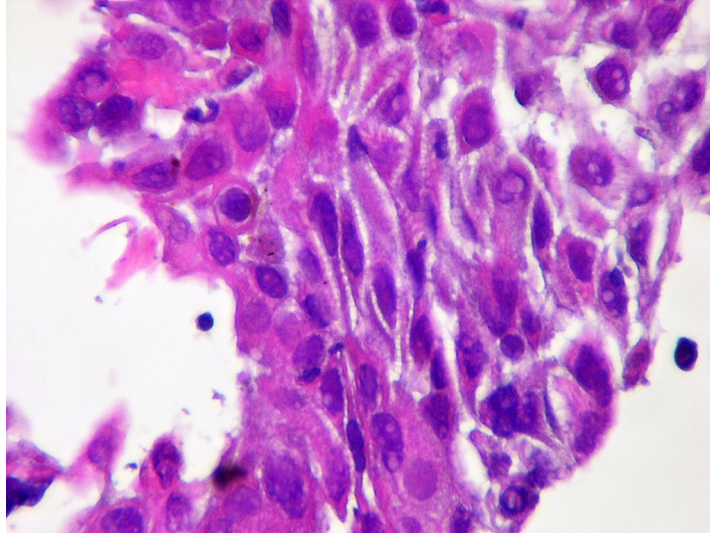
Figure 2.4: Squamous cell carcinoma [12].

- **Neuroendocrine carcinomas (NEC)** are lowlily differentiated high-grade malignant carcinomas.

- **Mixed neuroendocrine-nonneuroendocrine neoplasms (MiNEN)** are combined tumors with morphologically different cancer tissues.

Small cell neuroendocrine carcinoma is a highly malignant type of epithelial tumor, which makes up for up to 20% of all lung tumors. Because of the relatively small size of the carcinomas, small cell carcinomas are diagnosed in advanced stages. These cells produce active neuroendocrine substances that can cause paraneoplastic symptoms. Carcinomas create cell masses at the lung hilus and metastasize in mediastinal lymph nodes. Cells are mitotically active and often cause necrosis of the tissue. Small cell neuroendocrine carcinoma can be isolated or can be a part of a large cell neuroendocrine carcinoma.

Large cell neuroendocrine carcinoma is very similar to small cell neuroendocrine carcinoma in terms of structure and malignity. The difference is that these carcinomas create large masses of tissue. Large neuroendocrine carcinomas need to be differentiated from non-neuroendocrine carcinomas. If diagnosed in the early stages, surgical removal of cancerous tissue is possible. [29, 28]
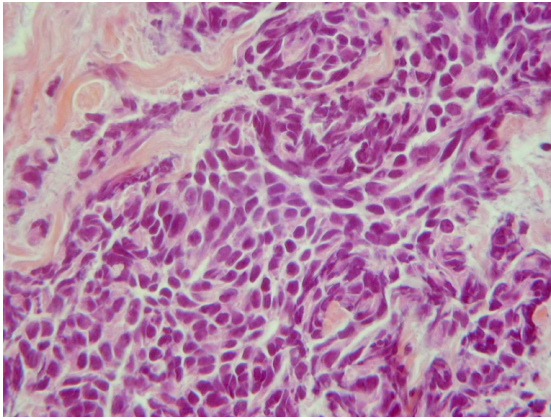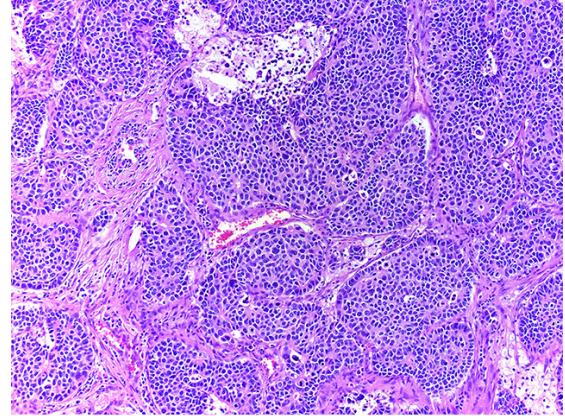
Figure 2.5: Small cell neuroendocrine carcinoma [11].

LCNEC H&E 100x

Figure 2.6: Large cell neuroendocrine carcinoma [7].

2.2.4 Large cell carcinoma

Large cell carcinomas create sizeable masses of unidentified cells with larger amounts of cytoplasm. They are comprised of large, undifferentiated tumor cells arranged in nests or sheets. They appear firm, flashy, and tan-white. If a given tumor does not meet the requirements for other types of carcinomas, it is designated as large cell carcinoma. [29][28][3]
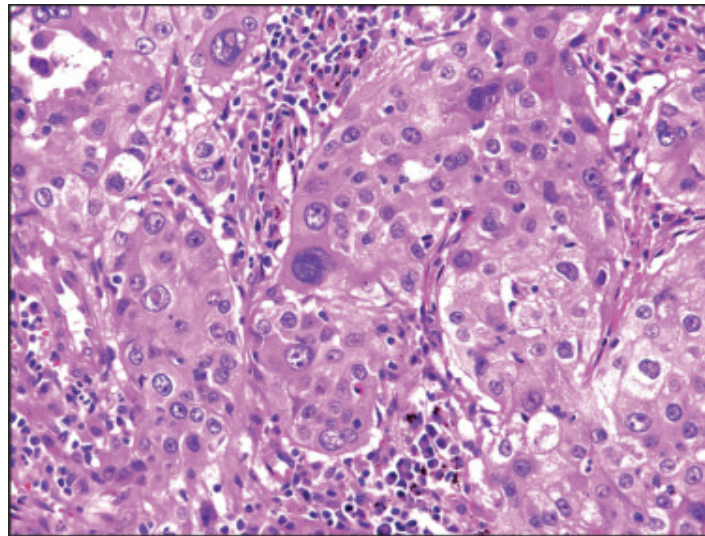

Figure 2.7: Large cell carcinoma [4].

Chapter 3

Current medical imaging

This chapter will discuss current medical imaging techniques used for lung screening and detection of pathologies. Many of these come with a number of complications, and not all are ideal for quick, on-site screening examination. [16]

3.1 Ionizing and non-ionizing radiation

In medical imaging, a system makes use of energy produced by an outside source to create a final image. This energy is transmitted in the direction of the target, and depending on the harmfulness of this radiation, we distinguish two types of radiation. [16]

3.1.1 Ionizing radiation

Ionizing radiation is used in a number of modern imaging systems and is still heavily relied on since it allows medical personnel, to a certain degree, examine the insides of a human body with a reasonable degree of image detail. In medicine, the most common type of ionizing radiation are **x-rays**. Depending on the used apparatus, images created using ionizing radiation can be summation images (projection radiography, positron emission tomography) or three-dimensional images created from multiple two-dimensional transverse scans (computed tomography). [16]

, However, ionizing radiation causes harmful effects on the human body due to its high energy values. When passing through the body, beams of energy interact with atoms in various tissues. Electrons orbiting around their nuclei are bound to them by **bounding energy**. When x-rays interact with these electrons, their energy can force these electrons to eject from their orbital position. This damage negatively affects an organism's cell composition. These impacted cells can be eliminated by the immune system. However, if these damaged cells are allowed to propagate, they can possibly differentiate into malignant cells and cause cancer. [23, 16]

Depending on the scanned area, different parameters have to be set for the imaging to be effective and, therefore, can increase the x-ray dose required. The amount of radiation received can range from 0.001 mSv **(x-ray imaging of extremities)** to about 22 mSv **(Positron Emission Tomography - Computed Tomography or PET-CT)**, which is an amount a person would receive from background environment in roughly 3.3 years. [10, 16]

3.1.2 Non-Ionizing radiation

In comparison to ionizing radiation, non-ionizing radiation does not carry enough energy to cause cell damage and therefore is generally safe to use for prolonged periods of time. These imaging systems usually have only enough energy to bring atoms to a higher energy state but do not cause any electrons to eject from their orbital positions. Systems included in this category make use of **infrared** (infrared cameras) and **visible** (endoscopes) electromagnetic spectrum, as well as **radiowaves** (magnetic resonance). [16]

While not using any type of electromagnetic radiation, **ultrasound imaging** can be included in this category, as it is mostly harmless to the human body and allows for safe imaging of delicate body parts or fetuses. [16]

3.2 X-rays

The first use of x-rays for medical imaging was documented in 1895 when Wilhelm Conrad Röntgen first used them to create an x-ray image of his wife's hand. Nowadays, x-rays are still widely used for diagnostic purposes, and about 3.6 billion diagnostic medical examinations are performed every year. [13] Medical specialists are able to determine the adequate dose of radiation needed for a procedure and, therefore, lower the possibility of health hazards. Basic x-ray imaging systems are also cheap and are widely accessible in modern countries. [16]

3.2.1 X-ray production

As the x-rays are part of the electromagnetic spectrum, they are produced by high-energy electron interaction with matter, releasing some of its energy as electromagnetic radiation. The individual parts that take part in this production are housed in an **x-ray tube**. This tube contains a high voltage source, an anode, a cathode, and a target electrode, all housed in a vacuum tube. [16]

The cathode is heated to high temperatures and undergoes thermal ionization, essentially freeing electrons. Opposite this cathode is an anode with a target electrode placed onto it. When cathode electrodes are ejected from their orbital positions, they are accelerated by the potential difference between the cathode and the anode and coming into contact with the target electrode. Depending on the type of interaction with the electrode, we distinguish two types of produced x-rays:

- **Bremsstrahlung spectrum** is a continuous spectrum of electromagnetic radiation. When an accelerated electron comes into contact with the electrode's nucleus, its energy is released. Comparatively, if the electron does not come into direct contact, but only passes the nucleus, a close or distant interaction can occur, altering the electron's travel path and releasing some of its energy. Because the amount of radiation generated is dependent on the interaction distance, Bremsstrahlung Spectrum is a continuous spectrum of electromagnetic radiation. [16]

- **Characteristic x-ray spectrum** is a discrete spectrum of electromagnetic radiation. Unlike the Bremsstrahlung Spectrum, a characteristic x-ray spectrum is produced by the interaction of the accelerated electron and an electron in the target electrode. When an electron is ejected from its orbital position around the nucleus, another electron from higher orbitals takes its place. The energy difference between these two
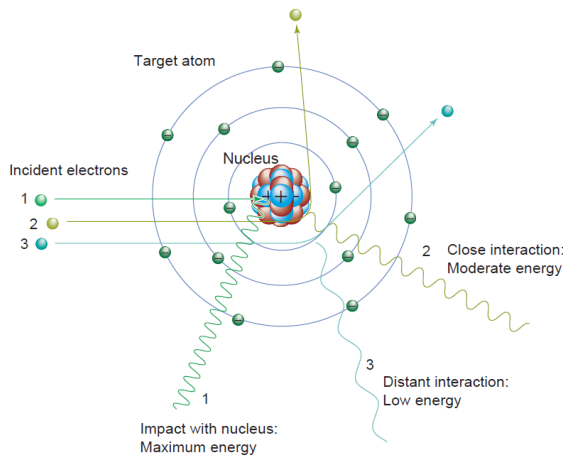
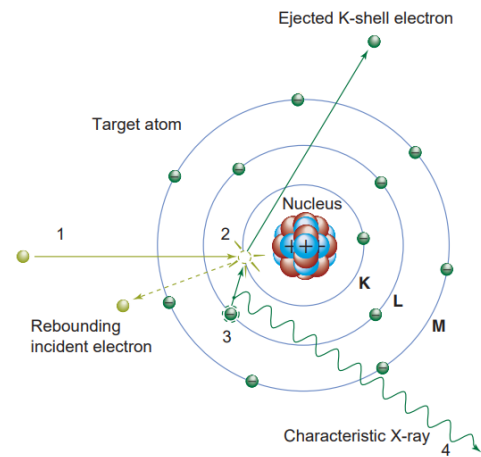Figure 3.1: Bremsstrahlung spectrum generation [16].

Figure 3.2: Characteristic x-ray spectrum generation [16].

orbitals is then released as characteristic radiation. It is a discrete spectrum, but the amount of energy released is different for different materials used. [16]

This radiation then passes through multiple filters and screens and then through a scanned body part, landing on a detection panel underneath the patient. Depending on the structures these x-ray beams pass through, they are more or less absorbed, resulting in the final image. [16]

3.2.2 Factors

X-ray systems can be adjusted in different areas, which, when properly tuned, can significantly lower the patient's received dose of radiation. Depending on the scanned body part, factors that can be adjusted are:

- **Tube voltage** alters the spectrum of x-ray photons and affects both the quantity and quality of photons. As the potential difference between the anode and the cathode increases, the speed of electrons ejected from the cathode increases as well. It also changes the spectrum of the incident photons, as it increases photons' maximal and average energy. [14] This lowers the required exposure time needed for a single scan, thus reducing the dose for the patient. However, it negatively affects the resultant contrast in the image, as higher voltage also increases the ratio of negative interactions with the tissues, creating image noise. In order to avoid unnecessary long exposure times when it comes to scans of thicker body parts, increasing the tube voltage is preferred, as the lower dose is prioritized over higher contrast.

- **Tube current** gives the number of electrons flowing from the tube in a unit of time. With higher amounts of x-ray photons, negative x-ray interactions affect the resultant image less. A smaller number of photons landing on the detector means that the detector has less exposition, lowering the contrast. However, increasing the value of tube current increases the dose for the patient as well, as doubling the tube current means doubling the dose for the patient. The tube current does not affect the energy of photons, only their overall amount.

- **Exposure time** is a time for the duration of which a patient is exposed to x-ray radiation. The tube current and the tube voltage have to be adjusted properly to achieve the best exposure time for the given application.

- **Source-to-image ratio**, which is standardized to 100cm or 183cm for chest radiography. [16]

3.2.3   Projection radiography

Projection radiography is the most basic diagnostic procedure using x-ray beams. A patient is placed in front of a detection screen, and x-ray beams are emitted from an x-ray tube in the patient's direction. Depending on the types of tissue encountered by the x-rays, they can be absorbed or pass through the matter relatively unchanged. This absorption is dependent on the atomic number of the material compounds the beams are passing through - the higher the number, the higher the absorption. [17] Therefore, high-density tissue, like bone tissue, will not allow a large dose of an x-ray to pass through, resulting in a white color x-ray image. On the other hand, lungs are shown to be of dark colors, as they are mostly filled with air. This trait is useful in detecting bigger anomalies in the lung area, as they will show up as brighter areas.
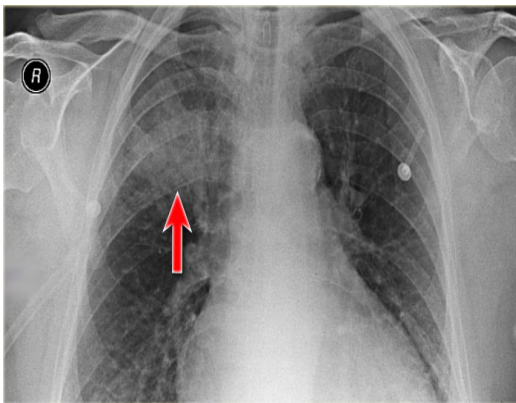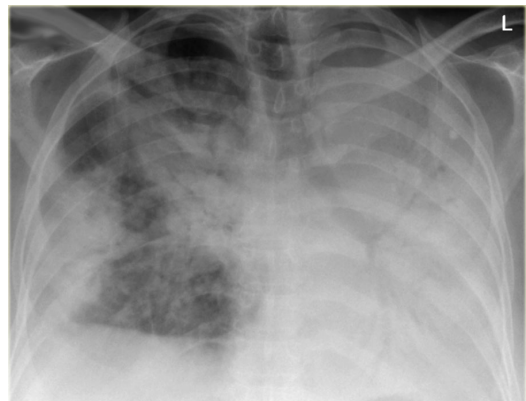

Figure 3.3: Lobar Pneumonia [5]

Figure 3.4: Diffuse consolidation in bronchoalveolar carcinoma [2].

3.2.4 Computed tomography

Computer tomography allows for the creation of transversal scans of human bodies using back projections. A patient is placed on an adjustable table, which can move depending on the desired range of body scans. The patient is then moved through a circular computed tomography scanner. This scanner is a rotating x-ray tube that periodically creates x-ray images around the patient. All images created from one 360-degree rotation are then reconstructed into the final transversal slice image. Because of this, the general amount of radiation dose is higher than the amount received during normal chest radiography. [10]

In modern computed tomography systems, the patient table is continuously moved through the rotating gantry, creating a helix around the patient. The pitch gives the distance covered by the computed tomography scanner per rotation. With a default pitch value of 1, a continual helix shape is created with no gaps. Changing this value depends on the application. Decreasing the pitch will cause the individual 360-degree scans to overlap, increasing the dose for the patient as the tissue is irradiated more per scan. This is useful in cases of obese patients. With higher pitch values than 1, there will be gaps in the helix, resulting in a lower dose and lower image quality, as the body parts will not receive a full 360-degree scan. These are useful for quick scans, where low radiation values are preferred. For cardiac applications, computed tomography systems are connected to an electrocardiogram machine and only scanning during certain intervals in cardiac activity. [16]

As mentioned before, in order to create an image, the individual scans, or **projections**, have to be reconstructed. By rotating the scanner around the patient, a set of forward projections are created in a 180-degree range. These values are stored in a sinogram, a histogram with angle specification. By using **back projection**, we can project individual projections into an image matrix in respect of the angles they were taken under. However, such reconstruction only yields blurry images and does not offer the required level of detail. As such, this sinogram data has to be filtered. In basic, this filter is called a **RAMP filter**, and many other filters incorporate this filter in themselves in order to minimize the negative effects of the RAMP filter. The frequency response of this filter is $|\omega|$, which is basically a multiplication on a frequency domain. By using this method, the resultant sinogram is filtered and provides a much clearer reconstructed image. This method is called a **filtered back projection**. [16]

Nowadays, computed tomography systems use **Iterative reconstruction** to reconstruct the final image. Iterative reconstruction has not been a possibility in the past, as the size of today's computed tomography scanning matrixes is about 512x512, which makes it very numerically intensive. Iterative reconstruction iterates a series of projections and makes use of forward projections and measured projections to minimize the error matrix, which is a matrix created from the difference between forward projection and measured projection. When the error matrix is minimized to a certain point, the computed tomography image should represent the object scanned. [16]

Computer tomography increases the detection rate of small nodules (less than 5mm in diameter), as specialists can examine multiple slices of the chest cavity. These small nodules can be missed in normal chest radiography because of the summation projection. The ability to reconstruct a three-dimensional image from the slices is shown to improve the detection of pleural invasion. [20]
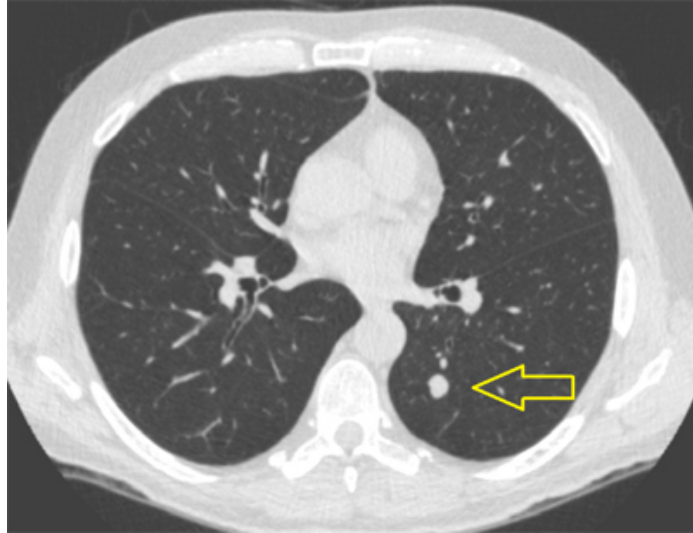
Figure 3.5: Lung nodule. [6]

3.3   Ultrasound

Unlike x-rays, which are a form of electromagnetic energy, ultrasound waves are a form of mechanical energy. Ultrasound is a sound with a very high frequency, generally above 20 kHz. High-frequency ultrasound, with frequencies from 1 MHz to 40 MHz, is used for diagnostic purposes in medical imaging systems. [16]

3.3.1   Principle

Ultrasound imaging systems make use of the ultrasound's properties when generating images of internal body structures. These systems make use of piezoelectric ultrasonic transducers to generate ultrasound waves, which travel at a speed of sound. While the pulse travels through the tissues, a portion of its energy (an echo) is reflected back to the transducer. Depending on the amplitude and the time difference between the initial pulse and the echo registration on the transducer, we can determine what kind of tissue the echo represents and its depth in the body. These pulses are then rapidly repeated with minor adjustments to the direction. Acquisition of these echoes over a period of time is used to reconstruct the final topographic image. [16]

When sound is generated, it moves through a medium by compression and rarefaction of particles in the medium. Therefore, the properties of sound depend not only on the properties of the source but also on the properties of the medium the sound propagates through. In the case of ultrasound imaging, the density and elasticity of different mediums affect the properties of the echo registered by the transducer. [16]

Different properties of sound affect how it interacts with the mediums it passes through:

- **Frequency** indicates how many times a wave oscillates in a unit of time.

- **Wavelength** is a distance between any 2 points on a sinusoidal wave with the same value.

- **Speed of sound** is a distance traveled by a sound wave in a unit of time.

High-frequency sound waves have lower penetration values in a unit of time due to smaller wavelength but offer a higher spatial resolution. Therefore, ultrasound frequencies are chosen depending on the body part. For areas that are situated deeper in the body, lower frequencies with longer wavelengths are used. On the other hand, for organs situated closer to the transducer, high frequencies with shorter wavelengths can be used for better spatial resolution.

As the sound travels through the medium, its interactions with the medium are influenced by the acoustic properties of the medium. Mainly, reflection is the main source of the echo that is reflected back to the transducer. The amount of reflected energy is directly affected by the **acoustic impedance** of interfacing mediums' materials. As mentioned before, the stiffness and density of a medium directly affect the sound waves. Mainly, a large difference in acoustic impedances between two different tissues greatly reduces the intensity of a sound wave traveling through the tissues. It is for this reason that cranial ultrasounds are very difficult to perform, as the human skull is very dense and stiff. On the other hand, because lungs are filled with compressible air, lowering the speed of sound. Even more, because of the large acoustic impedance difference between the lung tissue and the air in the lungs, any ultrasound wave emitted in this direction will be reflected. In order to reduce the effects of air on ultrasonic waves, medical personnel apply an ultrasound gel, which serves as an acoustic couplant through which the ultrasound waves can propagate, reducing the difference in acoustic impedances. [16]

Similar to reflection, refraction is an interaction between the sound and a tissue boundary. While some of the energy is reflected, some continue to propagate into another type of tissue. If the incident sound beam is perpendicular to the surface of this boundary, a portion of the energy is reflected in the opposite direction of the incident beam. In the case of a non-perpendicular beam, reflection happens at an angle that is equal to the angle of the incident beam. The energy that continues to propagate is then refracted under an angle that is determined by the speed of sound change on the boundary and the incidence angle. [16]

Scattering occurs when the ultrasound's wavelength is bigger than various objects within a tissue. These are called non-specular reflectors. Non-specular reflectors reflect incoming waves in multiple directions, and the amplitudes of these non-specular reflections are drastically reduced. These low amplitude reflections correspond to brightness changes in the final image. [16]

3.3.2   Transducer

Ultrasound waves are generated using piezoelectric crystals. In the event of crystal deformation, a slight electric charge is created on the surface of the crystal **(Direct piezoelectric effect)**. However, in the reverse event, when the surface of the crystal is subjected to an electrical charge, crystal deformation occurs **(Inverse piezoelectric effect)**. Both of these effects are used in ultrasound imaging. When short bursts of electric impulses are applied, the piezoelectric crystals vibrate on resonance frequencies, creating sound waves. Materials used for these transducers are usually natural crystals (quartz, tourmaline) or artificially created crystals (lithiumsulfates or piezoceramics). [16]

Ultrasound probes function in 2 modes, transmission, and reception. During transmission, an ultrasound probe sends out ultrasound waves, while during the reception, the probe detects waves reflected from body structures.
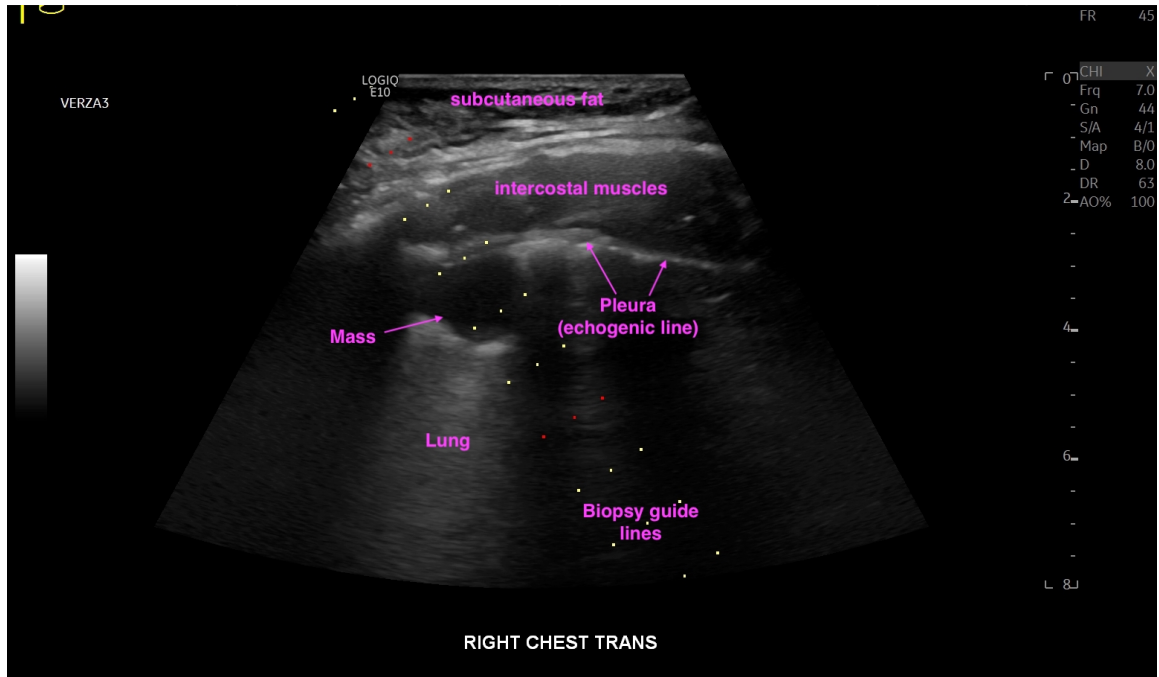
Figure 3.6: Lung ultrasound [19]

3.4 Nuclear medicine

Nuclear medicine imaging systems use radioactive materials to visualize activity inside a human body. As diagnostic radiopharmaceuticals are given to the patient, they emit photons in all directions. These photons are then detected on detectors, creating a heat map of the localization of the diagnostic pharmaceutical. Nuclear medicine imaging systems are useful for the detection of myocardial ischemia, tumors, or bone disorders but are especially useful for monitoring brain activity during different psychological responses. [16]

3.4.1 Diagnostic radiopharmaceuticals

Diagnostic radiopharmaceuticals are radioactive materials that decay inside of the patient and emit gamma or x-ray electromagnetic energy, which is used for the creation of diagnostic purposes, showing the distribution of radioactive material inside the patient. These diagnostic radiopharmaceuticals must have a reasonable decay time. If this decay time is too short, it will not allow for adequate image acquisition. On the other hand, if the decay time is too long, it may endanger the health of the patient because of the ionizing radiation produced. Various radiopharmaceuticals have different organ affinities, so the option depends on the procedure. If the diagnostic radiopharmaceutical is condensed in a particular area and behaves differently than expected, nuclear medicine systems can detect this phenomenon and show it on the resultant images. [16]

Depending on the procedure and used diagnostic system, different diagnostic radiopharmaceuticals decay, releasing different energy. As mentioned before, some diagnostic radiopharmaceuticals decay and release gamma and x-ray electromagnetic radiation, which are then caught on detectors. These are used in **Single photon emission computed tomography (SPECT).** However, in the case of **Positron emission tomography (PET)**,

diagnostic radiopharmaceuticals decay, releasing positrons, which then annihilate, releasing gamma radiation in opposite directions. [16]

3.4.2   Single photon emission computed tomography

As mentioned in the section above, single-photon emission computed tomography uses electromagnetic energy from decaying diagnostic radiopharmaceuticals to observe the physiological activity of internal organs. Similar to x-ray computed tomography, single-photon emission computed tomography creates a transverse image from multiple projections taken from different angles around the patient.

Because single-photon emission computed tomography cameras have multiple rows of detectors, this allows for volume data acquisition and the creation of transverse images of the entire field of view. These cameras can function in continuous mode when creating projections, or they can acquire data in set spaced angles around the patient („step and shoot"). For most cardiac procedures, the single-photon emission computed tomography camera only makes a 180-degree arc around the patient, as the attenuation of electromagnetic energy is lower from the frontal side of the patient. This is because the photons do not have to pass through multiple layers of body structures when captured from the front. This can result in higher spatial contrast in resultant images, and in case of need, single-photon emission computed tomography systems can substitute for missing projections from the other side of the patient by mirroring already acquired images. For non-cardiac procedures, usually, the whole 360-degree orbit is utilized. [16]

As mentioned before, as electromagnetic photons travel through body structures, they are attenuated in a different way depending on the distance traveled through the body. This attenuation is non-uniform and single-photon emission computed tomography systems have to account for this attenuation in the construction of the final image. A number of single-photon emission computed tomography systems use a second source of electromagnetic energy to measure the degree of attenuation at different angles around the patient. This measurement is done during the actual gathering of emission data from the diagnostic pharmaceuticals, as doing it separately would greatly increase the acquisition time. Single-photon emission tomography cameras, therefore, have two types of scintillators that react to different energy photons. These attenuation measurements are then later used during image reconstruction for attenuation correction. [16]
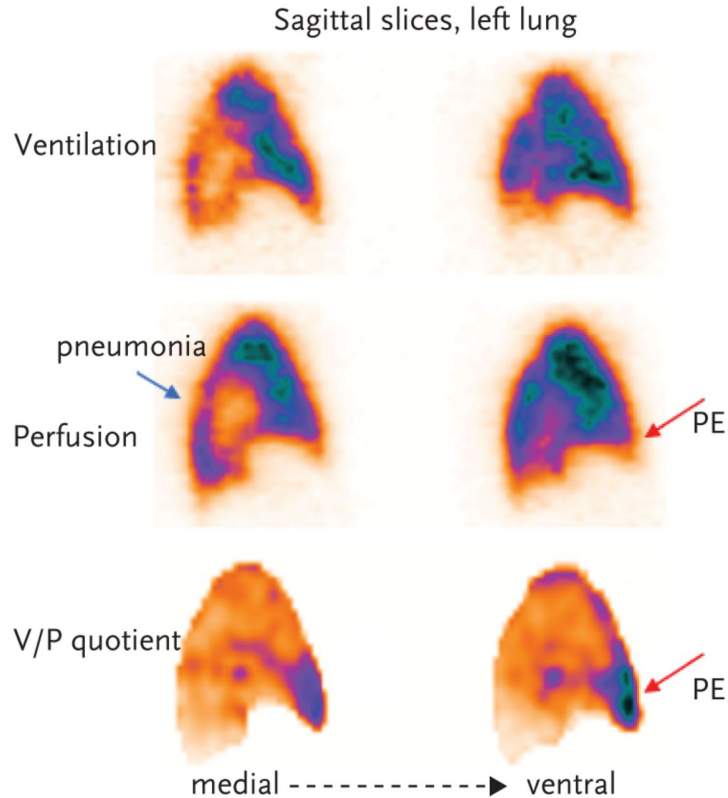
Figure 3.7: Lung SPECT scan [15]

3.4.3 Positron emission tomography

Positron emission tomography uses positron annihilation detection to observe physiological activity in internal organs. Unlike single-photon emission computed tomography, positron emission tomography does not use any rotating cameras to detect electromagnetic energy. Instead, similar to x-ray computed tomography gantries, scintillation detectors are housed in a large cylindrical gantry similar to x-ray computed tomography. [16]

In positron emission tomography, the patient is injected with diagnostic radiopharmaceuticals, most notably fluorine-18 fluorodeoxyglucose (FDG). Fluorine-18 fluorodeoxyglucose is a glucose analog and binds to red blood cells. However, unlike glucose, it is not metabolized, and unlike other diagnostic radiopharmaceuticals, it does not produce direct electromagnetic radiation after decay. Instead, it produces positrons, which are antimatter counterparts to electrons. Positrons travel through tissue, excite and ionize atoms and quickly lose energy. After their energy is spent, they interact with electrons and both annihilate, having their mass transformed into electromagnetic photons, which both have exactly 511keV and are emitted in opposite directions. These electromagnetic photons are detected by detector rings surrounding the patient, which use annihilation coincidence detection (ACD) to create projections of the diagnostic pharmaceuticals' activity. After a photon lands on a detector, the detector will not respond to other photons in order not to interfere with the reaction that is being processed at that moment. [16]

When an annihilation reaction occurs, three types of detections can occur:

- **True coincidence** happens when the two photons from the same annihilation reaction are detected at almost the same time. The computer then determines a line of

response between the two points of detection. These are the wanted interactions that create the diagnostic radiopharmaceutical distribution image. [16]

- **Scatter coincidence** occurs when a photon from an annihilation reaction is scattered in the body of a patient. These scattered photons can still be detector on the detector ring, thus creating a line of response that is not intersecting the point of annihilation reaction. This can contribute to spatial noise and artifacts in the resultant image. [16]

- **Random coincidence** is a coincidence where two photons from different annihilation reactions interact with the detectors at almost the same time. Similar to a scatter coincidence, this creates a line of response that does not intersect with the positions of original annihilation reactions and also contribute to the loss of spatial clarity. [16]

In order to reduce the effect of scatter and random coincidences, positron emission tomography systems can have collimators installed on top of their scintillation detectors. These collimators take the form of an axial septum, thin plates placed side by side that allow only straight traveling photons to reach the detectors. However, the collimators greatly reduce the number of detected photons. [16]

Similar to single-photon emission tomography and x-ray computed tomography, positron emission tomography uses filtered back projection or iterative reconstruction to create final, two-dimensional transverse images. Positron emission tomography systems are nowadays often used in conjunction with x-ray computed tomography to calculate the attenuation coefficient in different areas of the human body. [16]
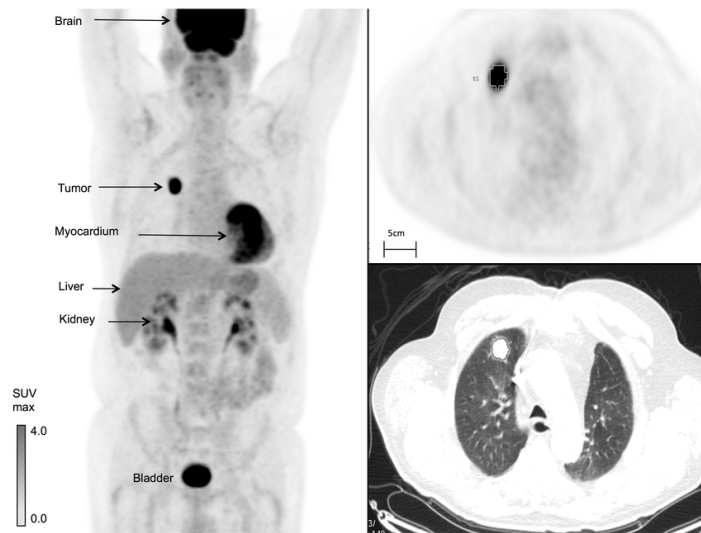

Figure 3.8: Lung PET scan [24]

3.5 Magnetic Resonance Imaging

Magnetic resonance imaging uses non-ionizing radiation to visualize the internal structures of a body. It uses a large, cylindrical magnet to create a magnetic field that makes free hydrogen atoms in the human body to along with it. Using radiofrequency pulses, these atoms are then flipped into high-energy states, and depending on their environments, they start to release their energy and return to the position that is parallel with the magnetic field

created by the magnet. The energy released is detected on magnetic resonance detectors and is used to create the final image. Hydrogen is used because of its paramagnetic properties and abundance in the human body. [16]

Under normal conditions, hydrogen atoms in the human body are not in phase due to the thermodynamic energy of their surroundings, spinning in various directions. Therefore, making the overall magnetic moment equal to zero. However, when placed into a magnetic field, these hydrogen atoms align with the field in parallel and antiparallel directions, with a slight majority being in the parallel direction. This creates a measurable net magnetic moment in the direction of the magnetic field. [16]

For imaging purposes, radiofrequency pulses are used to flip the directions of the precessing hydrogen protons from a parallel/antiparallel, longitudinal position into a transverse position perpendicular to the magnetic field. This pulse brings them into a high-energy transverse state. The most common pulse is a 90-degree pulse, but different degree pulses are also used to enhance the contrast of different tissues. From this excited state, hydrogen protons will start to relax and lose their energy. The rate of energy release is dependent on many variables, meaning that different tissues will have different energy signatures, allowing for differences in contrast.

We distinguish two different relaxation times:

- **T2 relaxation time** is a time for which it takes the protons' maximum transverse magnetic energy to reach zero. In the beginning, as all protons are in phase, the transverse magnetic moment is at its peak. Due to environmental inhomogeneities, protons in different tissues have different T2 relaxation times. Slowly, protons start to get out of phase, lowering the transverse magnetic moment. Structures containing molecules with a more unrestricted movement have less magnetic inhomogeneities in their environment, thus having long T2 relaxation times. On the other hand, hard stationary structures like bone tissue contain more magnetic inhomogeneities and have short T2 relaxation times. [16]

- The rotation of the transverse magnetic moment creates a sinusoidal signal induced on detectors. As the protons get out of phase, they cause a slow decrease in the overall amplitude of the rotating net magnetism. This signal is called a free induction decay, or FID. However, in reality, T2 is the decay time caused by protons' own magnetic inhomogeneities. However, T2* relaxation time is a T2 relaxation time that takes outside influences into consideration, therefore making T2* relaxation time shorter than the T2 relaxation time. [16]

- **T1 relaxation time** is a time for which it takes the longitudinal magnetization to recover 63% of its energy after a 90-degree flip. Unlike T2, T1 relaxation does not produce a magnetic resonance signal, thus has to be measured differently. After one 90-degree pulse is applied, the longitudinal magnetization is allowed to recover some of its energy, and after a set time delay, another 90-degree pulse is applied. This flips the recovered longitudinal magnetization into the transverse plane, causing a free induction decay. This process is repeated several times, and the peak amplitude measured after these flips is recorded and used to estimate the T1 relaxation time. T1 relaxation times are longer than T2 relaxation times and depend on tissues' energy dissipation characteristics. Materials, whose internal structure allow protons to tumble at Larmor frequency, show the shortest T1 relaxation times. The increased

strength of the induced magnetic field by the magnetic resonance magnet causes an increase in Larmor frequency, making T1 relaxation times longer. [16]
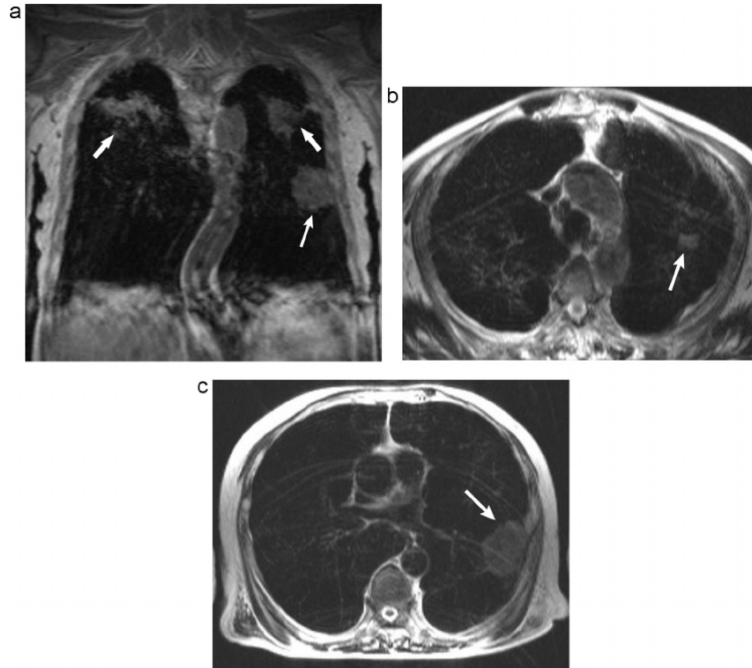

Figure 3.9: Lung MRI scan [15]

Image acquisition

As various tissues in the human body have different T1 and T2 relaxation times and proton densities, these variations can be used to enhance the contrast of structures we want to scan.

In order to work with these variables, a number of parameters can be set to target different tissues:

- **Time of repetition**, or TR, is the time difference between excitation pulses. As T1 and T2 relaxation times differ, so does the amount of energy released. [16]

- **Time of echo**, or TE, is the time between the 90-degree flip pulse and the peak amplitude of created echo. The echo is created by applying a 180-degree inversion pulse. [16]

- **Time of inversion**, or TI, is the time between the first 180-degree pulse and a 90-degree readout pulse. [16]

- **Partial saturation** is the level of magnetization. Tissue is unsaturated at its equilibrium, with its transverse energy being zero. After the first 90-degree pulse, the proton tries to return to its equilibrium state, but due to subsequent excitation pulses, it is never allowed to reach this state. After the second excitation pulse, the amplitude will reach less maximum value than before, as the longitudinal value did not reach its peak. After the third pulse, the speed of longitudinal recovery and transverse amplitude is constant, achieving a partial saturation, impacting tissue contrast. [16]

These parameters are used in spin-echo sequences, which are sequences of 90-degree excitation pulses and 180-degree refocusing pulses. By applying 90 and 180-degree pulses in varying times based on these parameters, we can achieve different contrast between tissues with different characteristics: [16]

- **T1 weighting** emphasizes T1 relaxation times to produce contrast. The differences can be maximized by using short TR and TE times, making structures with fast T1 relaxation times release more energy due to frequent excitation pulses. [16]

- **Proton density weighting** emphasizes differences in amounts of magnetized protons in tissues, as more magnetized protons mean larger longitudinal magnetization. Proton density weighting uses long TR times and short TE times to minimize the effects of T1 and T2 relaxation times. [16]

- **T2 weighting** emphasizes T2 relaxation times. It has long both TE and TR times to minimize T1 relaxation time differences and to allow for maximal T2 transverse relaxation. Long TE times allow for larger amounts of energy to be released. [16]

Chapter 4

Input acquisition setup

Unlike previously discussed imaging systems, the input images and videos used for this work have been acquired by using pulmonary endoscopy. Using this method allows for real-time visualization of lung tissue and possible performance of biopsy guided by this endoscopy. Nowadays, such biopsies are performed while guided by ultrasound imaging or while guided by computed tomography system. Pulmonary endoscopy relieves the patient of harmful radiation, as it only uses near-infrared light to illuminate the bronchi. It is also more accessible, as it does not require specialized equipment and provides reasonable localization of pathologies. [19, 22]

In this particular setup, a flexible endoscope was inserted into a patient via mouth with a near-infrared camera on its other end. Together with the endoscope, a near-infrared light-emitting diode, connected to a regulated power source, was inserted to provide a light source inside the patient and to transilluminate the lungs. With the near-infrared light being able to transilluminate the lungs up to a few centimeters into depth, it is possible to identify pathologies that would normally have to be discovered by other imaging technologies.

As discussed before, lungs and their pathologies undergo transformation into malignant tissue, their structures differ and therefore have different attenuation of light. This light scattering and attenuation will provide information about the type of tissue it is passing through, its structure, and other characteristics that can be used to distinguish between healthy lung parenchyma, cancer lesions, and other types of pathologies.

, However, as this setup is still in early development, it comes with drawbacks. As mentioned before, the near-infrared light-emitting diode is endoscopically inserted together with the flexible endoscope and has to be manually positioned into an adequate position in order to properly transilluminate the area that is captured by the camera. Because this near-infra red light-emitting diode can be classified as a point source of light, it can illuminate the area unequally, creating overexposed and underexposed areas, where discerning between tissue types is near impossible. Such conditions later cause complications to the illumination normalization algorithm, as it cannot properly adjust the values in the frame.

Figure 4.1: Image acquisition setup [15]

Chapter 5

Solution proposal and implementation

Overall, this application aims to be a diagnostics tool for medical personnel and provide analysis of prerecorded data. It applies an image processing algorithm consisting of illumination normalization and contrast limited adaptive histogram equalization to improve the clarity of an input image on which possible pathological areas are detected. These input and subsequent processed images are then shown side by side to the user. In the case of pathology detection, the image is saved into a save directory, and the user can open a new widget, where he can scroll through these saved images and review the detected pathologies.

5.1   Libraries and frameworks

As a programming language, C++ has been deemed the most suitable, as it provides reasonably fast execution speed and performance. Also, the libraries used in this program have sufficient C++ support and offer extensive possibilities in terms of algorithm and GUI design.

For image processing and recognition purposes, the open-source library OpenCV [1] is used in this work. OpenCV provides a large variety of different image processing functions that can be used to process and enhance bronchoscopy images, which is required to color-separate potential pathology sites from the non-pathological background. In this work, OpenCV is mainly used to mask pitch-black areas that provide no suitable information, such as the continuation of bronchus, so it does not interfere with dark area recognition. Secondly, it is used to enhance the visual quality of the image, allowing for better dark spot extraction. The program also uses OpenCV's BlobDetector to detect pathological areas, discerning between these depending on their size and circularity.

QT [2] has been used to create a simple GUI, as this program is aimed to be an analytical tool for medical personnel. QT offers easy to create user interface forms, paired with a C++ backend that is simple to connect with other before mentioned libraries.

---

[1] https://opencv.org/
[2] https://www.qt.io/

5.2 Image processing

5.2.1 Input frame

Before any computational image processing procedures, a region of interest, or ROI, is extracted from the input image. With the setup used to make recordings used as input in this work, the input frame size is 2048x1088 pixels. As our region of interest always occupies only the center portion of the frame, we can easily get the portion we need by creating a rectangle with fixed image coordinates and extracting pixels inside the rectangle.

Masking

In order to reduce false-positive detections, a mask has been created a mask in order to extract areas with a pixel value of zero and which, therefore, provide no information about the recorded tissue. If a pixel has zero value, it means that the tissue is not illuminated by the light source. The main reason for the mask is the continuation of the bronchial tube, which is not illuminated in its length, and therefore appears as a „black hole" in the frame.

The mask is created by thresholding the input image, masking away every pixel with zero value. Afterwards, the created mask is used to extract every non-zero pixel, therefore removing our „black hole." As a side effect, every other part of the image which has zero value pixels is masked away. However, this does not pose an issue, as such pixels are of no use. A bitwise-and operator is used to create the final masked image.
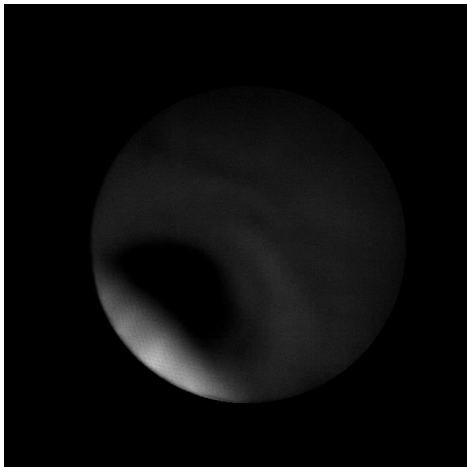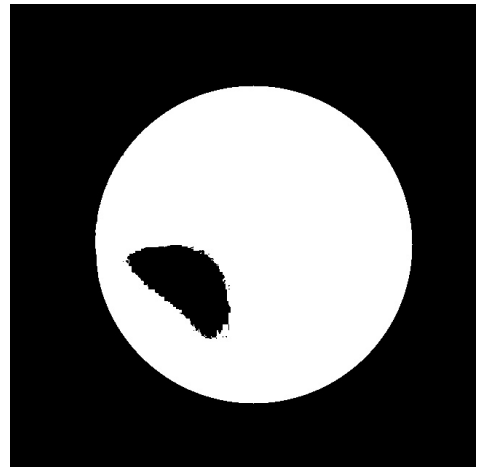

Figure 5.1: Input image.

Figure 5.2: Created mask.

Contrast enhancement and pathology detection

In order to better distinguish between pathological and non-pathological areas in the weakly illuminated frame, we have to make use of various image processing methods to normalize the illumination values in the input image. Therefore, an illumination normalization model has been implemented as following:

First, an estimation of local mean illumination has to be determined. This can be easily achieved by using a Gaussian filter with a sigma space value of 20. This has been experimentally determined to be the ideal value, as lower values do not produce sufficient image blurring. This mean illumination estimation matrix is later subtracted from the
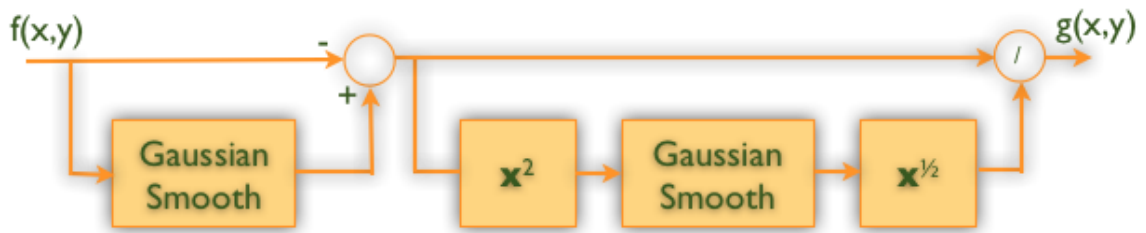
Illumination normalization model [25].

original input image, while slightly altering bright areas. Potential pathologies start to become more visible, but the overall illumination is still not normalized. This matrix is then squared, making the image generally darker.

Afterwards, using rooting operations on the last matrix, together with another Gaussian filter, a matrix with local variance estimation is created. By subtracting the local mean illumination from the input image and, subsequently, dividing this value by the estimation of local variance, we get an image with normalized illumination across the whole frame. In order to remove the black area around the bronchus, the before-mentioned mask is used to make the image clearer.

As can be seen in Figure 5.5, the rough outlines of potential pathologies are visible in the frame. The next procedure is smoothing this resultant image in order to remove any artifacts that could negatively affect image clarity. However, although this separation is better than in the input image, this can be improved upon using Contrast Limited Adaptive Histogram Equalization, or CLAHE. CLAHE equalizes the pixel values in a predefined square area, further enhancing the color separation between the pathological and non-pathological areas.
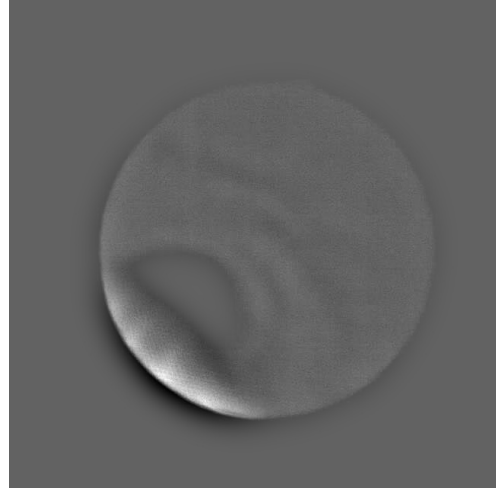
Figure 5.3: Estimation of local mean

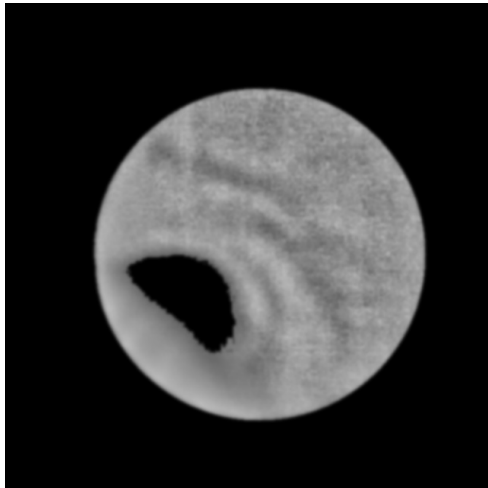Figure 5.4: Estimation of local mean subtracted
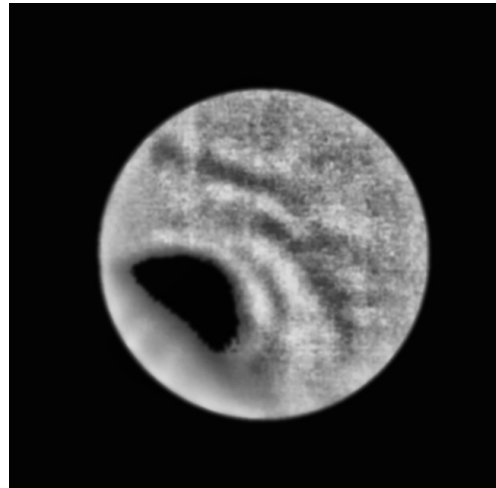

Figure 5.5: Enhanced

Figure 5.6: CLAHE

For pathology detection, the application uses OpenCV's BlobDetector. BlobDetector has a variety of different parameters that can be adjusted in order to maximize positive detection. BlobDetector detects dark areas, or „blobs,“ and saves the coordinates of the detected areas. These coordinates are then highlighted in the processed image for the user to see.

5.2.2 Graphical User Interface

As mentioned in the introduction to this chapter, this application should not only serve as a pathology detector but should also have a quality of life features that would make the use of this tool more pleasant. Therefore, a simple graphical user interface, or GUI, should be made to implemented to serve these needs.

Firstly, the main window of the GUI consists of two areas, where input and processed images are shown. The user can specify the input file by clicking on the button „Choose

file" a then navigating through directories. The selected file will then be processed frame by frame until the end, and the process can be stopped and resumed by the user anytime. A new file can also be selected while the old one is being processed.

Secondly, if the user wants to review frames with detected pathologies, another application window can be opened after clicking on the button „Saved pathologies." In this window, the user can select a folder with saved images, after which the content of the directory will be visible in a scroll area. The currently selected image in the scroll menu will be visible on the left side of the application window.

5.2.3 Implementation

Illumination normalization

As mentioned in Chapter 5, this application mostly uses data types included in OpenCV library. A variable of *cv::Mat*, representing a matrix, is created to store the image input, together with several other *cv::Mat* variables for subsequent processed images. *cv::Mat* stores every pixel value and is able to use arithmetic operations from standard C++ library to work with these values, such as *std::pow()*, which is used for illumination normalization. In order to perform these calculations accurately, matrixes are converted from single channel 8bit unsigned integer *(cv::CV_8UC1)* format to a single channel 32bit floating point *(cv::CV_32F)* format using *cv::convertTo()* function. The program performs all necessary operations described in the formula for illumination normalization and uses *cv::GaussianBlur()* to create the estimation of local mean and local variance. The masks are created using *cv::threshold()*, with the threshold value of 1, which makes every non-zero pixel white. After all the necessary image processing tasks, an object of *cv::SimpleBlobDetector* type is created, which is used to detect blobs in the image.
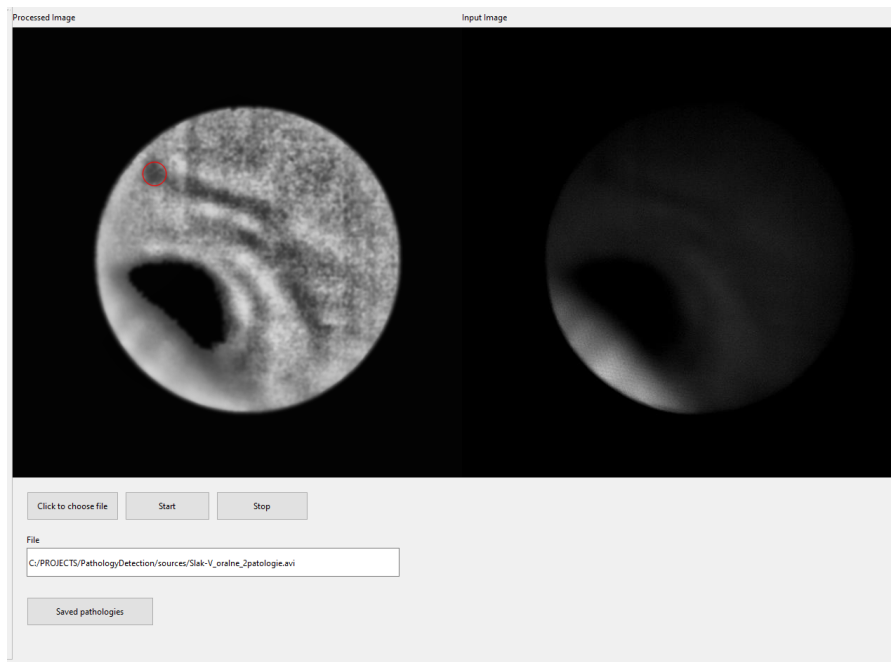

Figure 5.7: GUI

After the application starts, a main object of class *PathologyDetection* is created, whose class methods are responsible for running the entire application. After the initialization of this main object, a *QTimer* is set, which calls *PathologyDetection* class method *updateFrame*. Function *updateFrame* contains the functionality for image normalization and contrast enhancement, and returns a processed image. This processed image and the input image are shown side by side in two areas of type *QLabel* and are updated every time *updateFrame* is called.

By clicking on the button „Saved pathologies," the user can browse different directories with saved images containing detected pathologies. The contents of the directories will be visible in a scroll area.
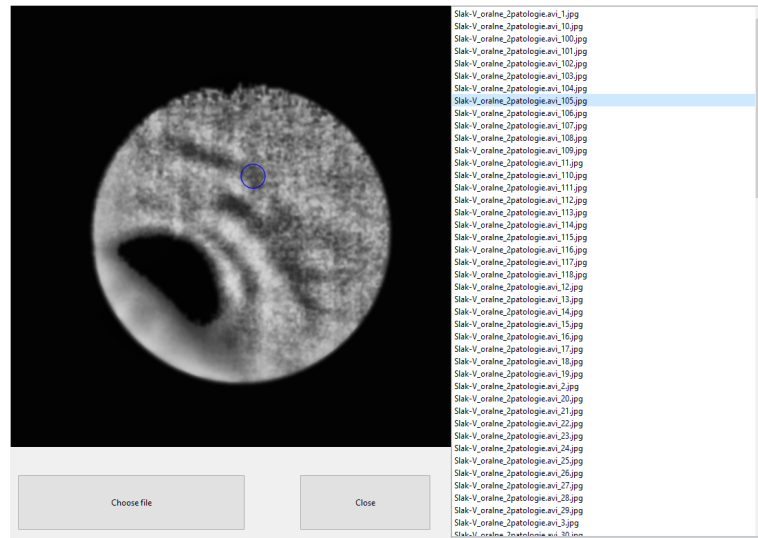

Figure 5.8: Image browser

Detection

As mentioned before, OpenCV's BlobDetector is used to detect pathologies. BlobDetector includes parameters that allow for better specifying the type of blob that should be highlighted. In this work, the only parameters used are *Inertia* and *Size.* Specifying the inertia values will make the detector highlight more elliptic blobs, while the Size parameter specifies the size range of the detected blobs. Using this, the detector should be able to discern areas that are not pathological but rather are shades created by the structure of the bronchi.

Chapter 6

Testing

Because of the experimental nature of both the image acquisition setup and the detection of lung pathologies, the testing of the application was performed with a very limited sample size of input videos. Generally, the algorithm performs the best when the scene is properly illuminated, and the camera is focused. Overexposure in one part of the image can cause slightly darker regions to be transformed into very dark blobs and, therefore, can be highlighted as pathological, while an unfocused camera creates a lack of structure definition. In this chapter, several images will be presented, with an input image on the right and a subsequent processed image on the left.
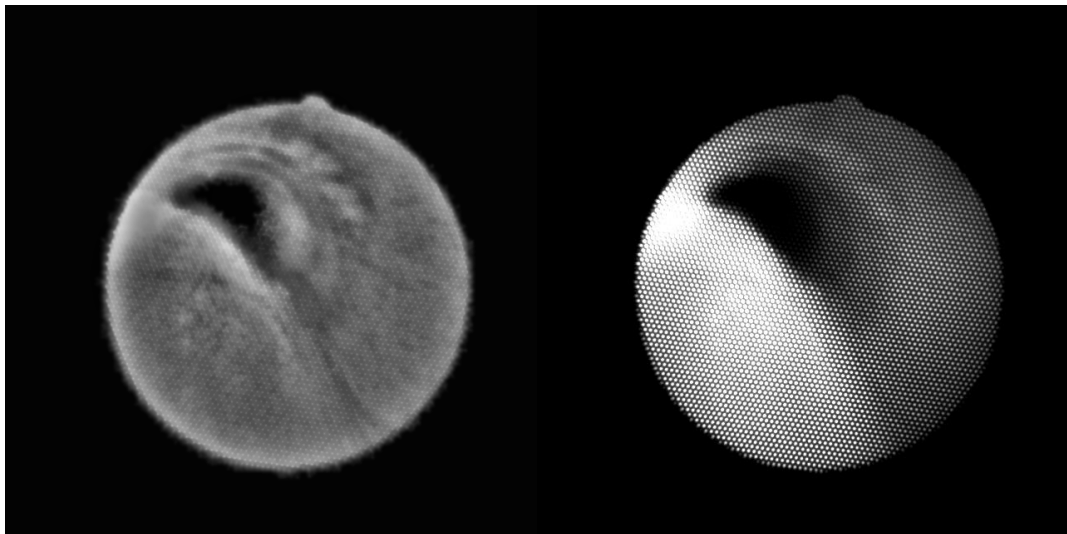

Figure 6.1:

Figure 6.1 presents an input image with optimal conditions, where the camera is focused, and the scene is not too overexposed. It is clear that after the image processing, the resultant image is much clearer than the input image, with better-differentiated structures and lines. The input image contains a mesh-like structure, which is caused by the construction of the fiber bronchoscope. The interference of the mesh is significantly lowered in the processed image. The input image contains some overexposure on the left side, however, it is not significant enough to hamper the image processing algorithm in a significant manner.
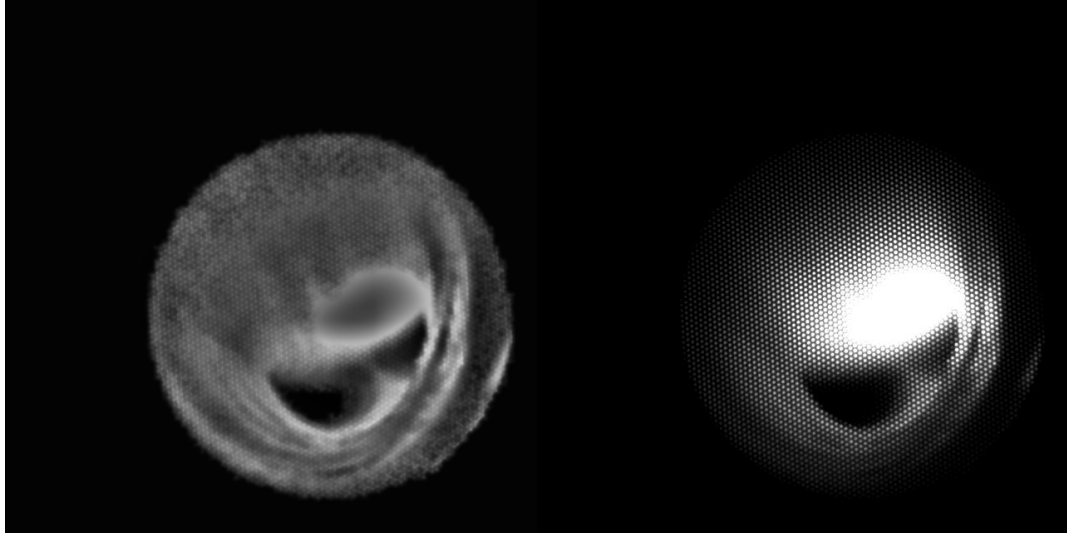
Figure 6.2:

Figure 6.2 shows slightly worse conditions. While the camera is properly focused, the frame is overexposed, with a very large bright spot in the middle of the image. Basic structures, like the bifurcation of the bronchi and folds on the bronchi surface are visible, the overexposure creates an imbalance in colors and increases the differences between light and dark regions. Also, the white spot lacks any type of definition and creates a large, grey blob.
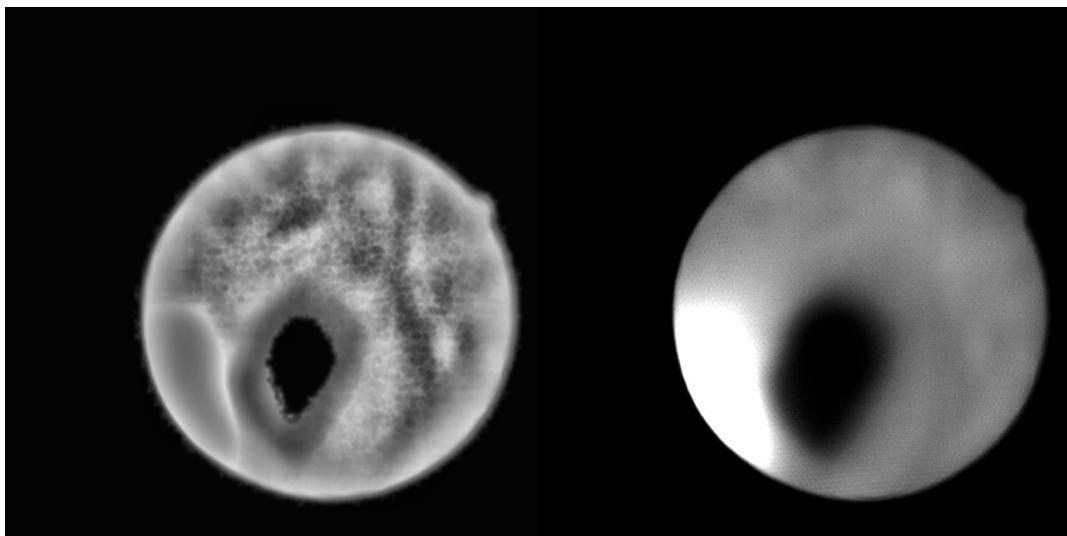

Figure 6.3:

Figure 6.3 presents largely sub-optimal conditions, where the input image is overexposed, with a bright spot in the lower-left quadrant and an unfocused camera. As described before, an unfocused camera causes a lack of structure definition, which can be seen in the input image, where only a slight semblance of dark lines can be seen. Due to these conditions, any darker spots are darkened even further to a point where they do not resemble

the original structures, and the processed images do not show any relevant information. Furthermore, these blurred, dark blobs can be falsely highlighted as pathological.
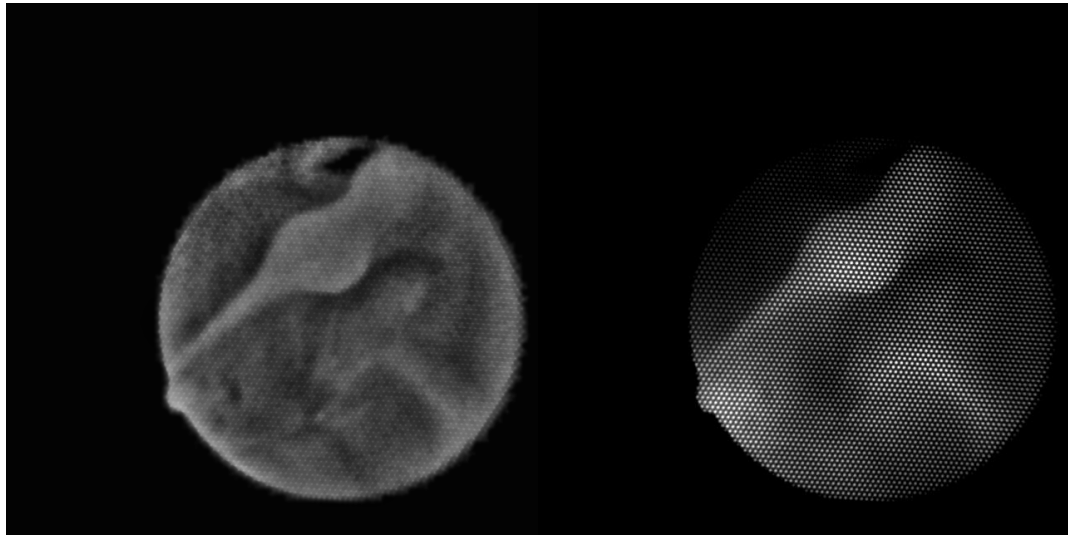

Figure 6.4:

In Figure 6.4, the input image contains a bronchial structure that stems from the surface of the bronchi and connects to the opposite side. As the structure grows into the space of the bronchi, it is better illuminated and positioned closer to the bronchoscope, the algorithm is not affected, and in the processed picture, the outer edges of the object are clearly visible, and the structure is distinguishable from the background.

Detection

Because the pathology detector works on the principle of detecting dark blobs, it is susceptible to errors due to the reasons described above. Even at optimal conditions, false-positive detections can still occur, as certain structures will resemble a shape of a pathology.
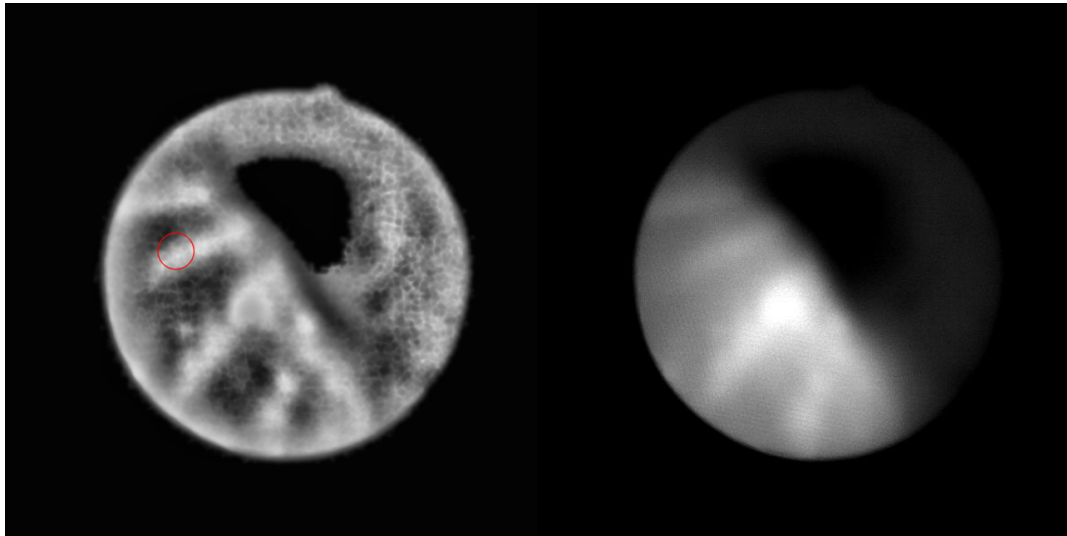
Figure 6.5:

Figure 6.5 shows an unevenly illuminated image with a small bright spot in the middle, as well as an unfocused camera. As can be seen in the processed image, ridges in the bronchial airways have been transformed into large dark areas, while in the input image, they are of a slightly darker shade of gray. This transformation triggers a false positive detection
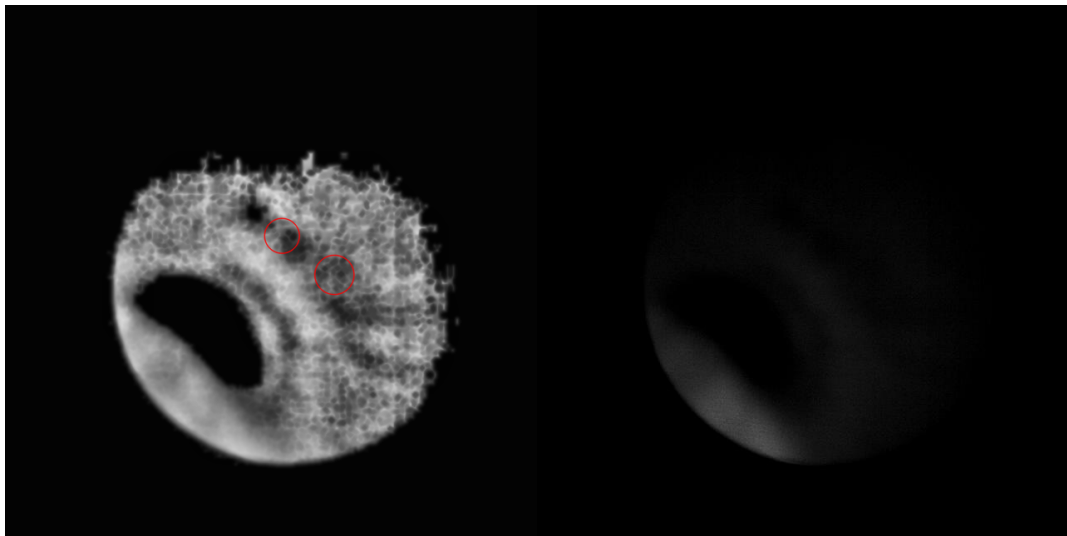

Figure 6.6:

In the input image of Figure 6.6, a pathology spanning the upper side of the bronchi sideways can be seen, with a smaller one behind it. These shades represent pulmonary nodules. While the camera is unfocused, the difference in color is great enough, and the pathology becomes visible in the processed image. This is a pathology and has been correctly highlighted by the algorithm.

Chapter 7

Conclusion

The aim of this work was to study various current medical imaging systems and image processing methods to create an algorithm for the detection of bronchial pathologies. The algorithm accepts video files as an input and processes them frame by frame, normalizing the illumination in each frame and highlighting possible pathologies. Input frames and processed frames are displayed to the user, and detected pathologies are saved for the user to review.

Limitations of this algorithm lie in the requirement of optimal conditions in the input image, as camera focus and illumination can severely interfere with the illumination normalization process and cause false-positive pathology detections. However, with optimal conditions, the algorithm provides a processed image with improved clarity and contrast. The detection method can be improved upon, however, it will require a bigger testing sample.

The algorithm for pathology detection shows promise, but work is still needed in order to better differentiate between pathological areas and areas that only resemble pathologies in their shape and color. This work provides a basic overview of the topic of bronchial pathology detection. In the future, multithreading can be implemented in order to speed up the image processing tasks, and new, improved detection methods based on feature matching can be made. With a big enough testing sample size, a neural network could be trained to detect pathologies instead of a parametric approach.

Bibliography

[1] *Anatomy of the Heart and Lungs.* [Online, accessed 19.1.2022]. Available at: `https://diagnosis101.welchallyn.com/wp-content/uploads/2018/06/` `WEL_10345_Diagnosis101_2-01-768x576.png`.

[2] *Diffuse consolidation.* [Online, accessed 19.1.2022]. Available at: `https://radiologyassistant.nl/assets/chest-x-ray-lung-disease/` `a50e999f9d1cae_3-diffuse-BAC.jpg`.

[3] *Large-cell-carcinoma.* [Online, accessed 19.1.2022]. Available at: `https://www.sciencedirect.com/topics/medicine-and-dentistry/large-cell-carcinoma`.

[4] *Large-cell-carcinoma.* [Online, accessed 19.1.2022]. Available at: `https://ars.els-cdn.com/content/image/3-s2.0-B9780123744197000184-f18-15-9780123744197.jpg`.

[5] *Lobar_pneumonia.* [Online, accessed 19.1.2022]. Available at: `https://radiologyassistant.nl/assets/chest-x-ray-lung-disease/` `a50e8490cad4c4__groot-cor-infi-rul.jpg`.

[6] *Lung Nodule Clinic.* [Online, accessed 15.1.2022]. Available at: `https://www.northlung.com/img/lung-scan.jpg`.

[7] *LungtumorlargecellNE.* [Online, accessed 19.1.2022]. Available at: `https://www.pathologyoutlines.com/imgau/lung-tumor/lungtumorlargecellNEwu05.jpg`.

[8] *Mucinous_adenocarcinoma_of_the_lung.* [Online, accessed 19.1.2022]. Available at: `https://commons.wikimedia.org/wiki/File:` `Mucinous_adenocarcinoma_of_the_lung_--_high_mag.jpg`.

[9] *Oxygen-dissociation.* [Online, accessed 19.1.2022]. Available at: `https://gpnotebook.com/resources/oxygen-dissociation%20curve.jpg`.

[10] *Radiation Dose in X Ray and CT Exams.* [Online, accessed 12.4.2022]. Available at: `https://www.radiologyinfo.org/en/info/safety-xray`.

[11] *Small-Cell-Neuroendocrine-Carcinoma.* [Online, accessed 19.1.2022]. Available at: `https://www.researchgate.net/profile/Pierre-Olivier-Vedrine/publication/` `7251318/figure/fig1/AS:` `277761357828098@1443234876469/Small-Cell-Neuroendocrine-Carcinoma.png`.

[12] *Squamous_cell_carcinoma.* [Online, accessed 19.1.2022]. Available at: `https://upload.wikimedia.org/wikipedia/commons/7/74/Squamous_cell_carcinoma_4.jpg`.

[13] *To X-ray or not to X-ray?* [Online, accessed 16.4.2022]. Available at: `https://www.who.int/news-room/feature-stories/detail/to-x-ray-or-not-to-x-ray-`.

[14] Ayush, G. and Joachim, F. *Kilovoltage peak.* [Online, accessed 20.4.2022]. Available at: `https://radiopaedia.org/articles/kilovoltage-peak`.

[15] Bajc, M. Potential of hybrid V/P SPECT–low-dose CT in lung diagnostics. *Breathe.* European Respiratory Society. 2012, vol. 9, no. 1, p. 48–60. DOI: 10.1183/20734735.018412. ISSN 1810-6838. Available at: `https://breathe.ersjournals.com/content/9/1/48`.

[16] Bushberg, J. T., Seibert, A. J., Leidholdt, E. M. and Boone, J. M. *The essential physics of medical imaging; 3rd ed.* Philadelphia, PA: Lippincott Williams Wilkins, 2012. ISBN 978-0-7817-8057-5.

[17] Griffith, J. F. and Genant, H. K. Chapter 64 - Imaging of Osteoporosis. In: Marcus, R., Feldman, D., Dempster, D. W., Luckey, M. and Cauley, J. A., ed. *Osteoporosis (Fourth Edition).* Fourth Editionth ed. San Diego: Academic Press, 2013, p. 1505–1534. ISBN 978-0-12-415853-5. [Online, accessed 19.4.2022]. Available at: `https://www.sciencedirect.com/science/article/pii/B9780124158535000649`.

[18] Hall, J. E. *Guyton and Hall Textbook of Medical Physiology.* 13th ed. Philadelphia: Elsevier, 2015. 497-549 p. ISBN 978-1-4557-7005-2.

[19] Hartung, M. P. *Ultrasound-guided lung nodule biopsy.* [Online, accessed 21.4.2022]. Available at: `https://radiopaedia.org/cases/ultrasound-guided-lung-nodule-biopsy`.

[20] Hollings, N. and Shaw, P. Diagnostic imaging of lung cancer. In: *European Respiratory Journal.* Lausanne: European Respiratory Society, 2002, vol. 19, no. 4, p. 722–742. ISSN 0903-1936. [Online, accessed 19.4.2022]. Available at: `https://erj.ersjournals.com/content/19/4/722`.

[21] Hudák, R. and Kachlík:, D. *Memorix anatomie.* 1st ed. Praha: Triton, 2013. 206-220 p. ISBN 978-80-7387-674-6.

[22] Kuriyama, T., Masago, K., Okada, Y. and Katakami, N. Computed tomography-guided lung biopsy: Association between biopsy needle angle and pneumothorax development. *Mol Clin Oncol.* Feb 2018, vol. 8, no. 2, p. 336–341.

[23] Land, C. *Ionizing radiation.* [Online, accessed 15.4.2022]. Available at: `https://www.britannica.com/science/ionizing-radiation`.

[24] Nair, V., Keu, K. V., Luttgen, M., Kolatkar, A., Vasanawala, M. et al. An Observational Study of Circulating Tumor Cells and F-FDG PET Uptake in Patients with Treatment-Naive Non-Small Cell Lung Cancer. *PloS one.* july 2013, vol. 8, p. e67733. DOI: 10.1371/journal.pone.0067733.

[25] Sage, D. and Unser, M. Easy Java Programming for Teaching Image Processing. In: *Proceedings of the 2001 IEEE International Conference on Image Processing (ICIP'01). Θεσσαλονίκη (Thessaloniki), Ελληνική Δημοκρατία (Hellenic Republic):* [b.n.], October 7-10, 2001, III, p. 298–301.

[26] Silbernagl, S. and Despopoulos, A. *Základy fyziologie*. 3rd ed. Praha: Grada Publishing, 2004. 106-138 p. ISBN 80-247-0630-X.

[27] Ward, J. P. and Linden, R. W. A. *Základy fyziologie*. 1st ed. Praha: Galén, 2010. 58-68 p. ISBN 978-80-7262-667-0.

[28] Zamecnik, J. and kolektiv. *Patologie 2*. 3rd ed. Praha: LD, s.r.o. - PRAGER PUBLISHING, 2019. 405-441 p. ISBN 978-80-270-6457-1.

[29] Zámečník, J. and kolektiv. *Patologie 1*. 3rd ed. Praha: LD, s.r.o. - PRAGER PUBLISHING, 2019. 229-263 p. ISBN 978-80-270-6457-1.

Appendix A

SD card content hierarchy

```
root
├── .vs/
├── doc/ .......Thesis text with source codes
│   ├── DetectionOfPathologiesInVideosFromBronchialPathways.pdf
│   └── src
├── application/ .........Executable application with libraries
│   └── PathologyDetection.exe
├── ImageBrowser.cpp
├── ImageBrowser.h
├── ImageBrowser.ui
├── main.cpp
├── MainController.cpp
├── MainController.h
├── PathologyDetection.cpp
├── PathologyDetection.h
├── PathologyDetection.pri
├── PathologyDetection.pro
├── PathologyDetection.qrc
├── PathologyDeteection.sln
├── PathologyDetection.ui
├── PathologyDetection.vcxproj
├── PathologyDetection.vcxproj.filters
├── PathologyDetection.vcxproj.user
```